2021

PERFORMANCE ASSESSMENT OF 3D PRINTED AUXETIC CEMENTITIOUS CELLULAR COMPOSITES

Nora-Kristin Kelter
University of Rhode Island, nora_kelter@uri.edu

PERFORMANCE ASSESSMENT OF 3D PRINTED AUXETIC CEMENTITIOUS CELLULAR COMPOSITES

BY

NORA-KRISTIN KELTER

A THESIS SUBMITTED IN PARTIAL FULFILLMENT OF THE

REQUIREMENTS FOR THE DEGREE OF

MASTER OF SCIENCE

IN

CIVIL ENGINEERING

UNIVERSITY OF RHODE ISLAND

2021

MASTER OF SCIENCE THESIS

OF

NORA-KRISTIN KELTER

APPROVED:

Thesis Committee:

Major Professor Sumanta Das

Aaron Bradshaw

Helio Matos

Brenton DeBoef

DEAN OF THE GRADUATE SCHOOL

UNIVERSITY OF RHODE ISLAND

2021

ABSTRACT

Auxetic behavior implies a negative Poisson's ratio whereby the specimen contracts instead of expands in transversal direction in a compression test. This novel response results from a special arrangement of voids formed by auxetic structures inside the sample. Combined with the advantages of concrete such as low costs, availability, strength in compression, durability, and fire resistance this innovative material of auxetic cementitious cellular composites (ACCC) provides a lot of new opportunities for the building industry. With the advent of 3D printing technology, it is now possible to achieve performance enhancement by tuning the geometrical architecture in the mesoscale. In this research different variations of auxetic mortar structures were investigated and a procedure to create auxetic test specimen was developed. New auxetic geometries applicable for a brittle material like mortar were generated. Molds with these structures were printed with a 3D printer to cast the mortar and after 28 days the samples were tested in compression and three-point bending tests. The digital image correlation (DIC) method was used to determine the displacements during the experiments as these are necessary to identify auxetic behavior. For this method a new technique including a handheld printer was developed to improve the procedure of painting the required black dots on the specimen. Analyzing the strength and auxetic behavior of the different structures, the modified re-entrant honeycomb structure was identified to be the most promising geometry for an application in the building industry. As a verification of the results and for defining requirements for auxetic behavior, FEA simulations were performed for CCCs with elliptical voids judiciously oriented to achieve auxetic behavior. The FEA simulation results suggest that a high number of elliptical voids and a long major

axis are necessary to achieve a negative Poisson's ratio. Besides, high aspect ratios of voids can enhance the auxetic behavior. The lowest Poisson's ratio found was -0.33 and the corresponding geometry can be used for future investigations. The discovered geometries can be used as a first step towards a varied and very auspicious application of ACCCs in civil engineering. The developed FEA-based simulation framework is used to generate a large, consistent dataset for auxetic CCCs with varying mesoscale architectural features. Such dataset can be leveraged to develop robust and efficient machine learning (ML)-based performance prediction tools in the future which would be of enormous value to the materials designers and decision-makers.

ACKNOWLEDGMENTS

First of all, I would like to thank my major advisor Dr. Sumanta Das for his support and mentorship during my research and for the opportunity to work on this innovative and interesting topic. I would also like to express my gratitude to Dr. Aaron Bradshaw for his decided commitment and effort, his moral support and for always expressing his faith in me. Furthermore, I want to thank my other committee member Dr. Helio Matos and my committee chair Dr. Sigrid Berka for making the graduation at the URI possible for me.

I owe significant gratitude to Gideon Lyngdoh and Sami Doner for introducing me to simulations and 3D printing, respectively, and for having been available whenever I needed their help. Gideon convinced especially with his general expertise and invaluable support for the paper. A special thank-you also goes to Sami and his cooking skills. I also want to thank Jonathan Villada for being a reliable lab mate and friend and for his positive energy and Sumeru Nayak for his helpful comments in our weekly research meetings.

In addition, I am indebted to the DAAD for his financial support and for offering this excellent Dual Degree program together with the TU Braunschweig and the University of Rhode Island. This year abroad was the best year I ever had.

I also want to thank my German and American friends for their support and trust in me and for distracting me whenever it was necessary.

A very big thank you goes to my parents. Thank you for your never-ending support and encouragement at any time and for your love and faith in me. I can’t thank you enough for giving me the opportunity of this year abroad.

Most importantly, I need to express my severe thank-you to my boyfriend Janis. Thank you from the bottom of my heart for your loving support, your never-ending motivation, and your ability to always stay positive. You never stopped believing in me and did more for me than I could ever verbalize. You've always been there for me and not only supported me morally, but you also helped me with ideas and supported me technically and in the lab with time-consuming tasks such as painting the cubes for the DIC method. Without you, I would never have made it and I am so thankful that we were able to share the experience of this year abroad.

TABLE OF CONTENTS

LIST OF TABLES

LIST OF FIGURES

CHAPTER 1

INTRODUCTION

Concrete is the most widely used material for construction purposes in the world owing to its good properties and relatively low costs [1, 2]. It is made by mixing coarse and fine aggregates and mortar, which is a combination of cement paste and sand. Concrete has a good compressive, but relatively low tensile strength [2]. Enormous studies have been investigated to improve the mechanical strength of the concrete such as adding admixture [3, 4] or fibers [5, 6] or changing the type of aggregates [7, 8]. Apart from modifying the material behavior, the mechanical enhancement can also be achieved from the structural behavior. For example, by optimizing the packing density of the aggregates [9] or modifying the air-voids [10, 11], the performance of concrete can be improved significantly. By changing the configuration of the so-called micro-structure or meso-structure of cementitious materials, a great improvement can be obtained.

An upcoming topic in research is the auxetic behavior of materials. The special feature of materials with this behavior is a negative Poisson's ratio that arises from a special arrangement of voids, that changes the micro-structure of the material. The Poisson's ratio is the relation of transverse strain to axial strain. In contrast to conventional materials with a positive Poisson's ratio, axial tension in a material with auxetic behavior leads to an increase in the cross-section, while axial compression induces a transversal contraction [12].

In this thesis, a concrete or cementitious cellular composite (CCC) with these new material characteristics will be generated. The objective is to achieve auxetic behavior on mortar samples tested in compression and three-point-bending tests. As auxetic CCC (ACCC) is still in its infancy, the auxetic structures for the mortar samples have to be modified from already existing auxetic structures for other materials. After that, molds for the mortar samples will be printed with a 3D printer and used for casting the specimen. After 28 days of hardening the samples will be tested for their compressive and flexural strength, respectively, and their auxetic behavior using the DIC method to determine the displacement of the test specimen during the experiment. In a final step the different auxetic structures will be analyzed for their strength and their auxetic behavior and compared to each other to determine their differences and their potential to be applied in the practice of the building industry.

So, the overall goals are to develop a procedure to create auxetic mortar samples, to find more auxetic structures that are applicable for concrete and to compare the experiment results of different structures to find the most useful ones, where useful not only means a negative Poisson's ratio but also a high strength in compression and bending.

CHAPTER 2

REVIEW OF LITERATURE

Compared to other building materials, concrete has several advantages including low costs, availability, strength in compression, durability, and fire resistance [1]. Nevertheless, the construction with conventional concrete is obsolete. Automation and digitalization for concrete structures are still in their initial stage whereas the construction with steel for example is much more advanced. Concrete requires significant time to develop to a fully-load bearing structure, it is not very precise, and it is challenging to construct a complex shape due to the need of framework. Furthermore, strenuous physical labor while using concrete in the building industry has caused significant health issues [1].

In contrast to conventional methods, a new innovative manufacturing approach for concrete components includes 3D printing. 3D printing is a new design method that enables a flexible shape, is cheap in production, less time-intensive, has better quality control and is much more automated which implicates less physical labor and more accuracy [13]. In ideal circumstances, the 3D printer directly prints the concrete out of its nozzle. However, due to some issues, for example with big aggregates in concrete, this technology is still in its infancy. Hence, instead of concrete, a cement paste without aggregates is used, which is then filled into 3D printed molds made of plastic like polylactic acid (PLA) with customizable geometry.

This new technology offers the possibility to create a material with completely new characteristics. The auxetic behavior occurs from the negative Poisson's ratio whereby the volume increases when pulling in contrast to materials with a positive Poisson's ratio because the material expands in all directions [12]. Auxetics were discovered in the 18th century in cat skin and a cancellous bone [14] and were named by Evans in 1991 [15]. There are different mechanisms to achieve auxetic behavior such as re-entrant honeycombs, rigid body rotation structures, crumpled or perforated sheet structures, chiral structures, folded structures, or buckling-induced structures [14–16]. These different structures that are used to create voids in the meso-scale implicate the degree of auxetic behavior of the whole component. Because of the unusual but desirable properties like enhanced indentation resistance, variable permeability, superior shear resistance, high fracture toughness, and damping and sound absorption [14, 16] auxetic materials are used for many different applications. These include but are not limited to sports and safety equipment, shock and sound-absorbing materials for vehicles and aircraft, seals, filters, prostheses, and textiles [12, 14, 16]. Regarding concrete in the building industry especially auxetic properties such as shear and indention resistance and damping and fracture toughness are helpful characteristics because they can improve the life-time and strength of the concrete component [13]. Therefore, the research in the field of auxetic cementitious cellular composites, which is the scientific name for the auxetic cement paste, can be a big step toward a successful, future-oriented, and diversified use of concrete.

Furthermore, there are some papers that illustrate the significance of research in this area. Researchers investigated in 2004 the bending behavior of a cantilever sandwich beam with auxetic core material in comparison to a cantilever sandwich beam with conventional core material. They discovered that the beam with auxetic core material deforms less than the one with conventional core material. This is due to a higher stiffness of the auxetic beam because it is more resistant to shear which is caused by the auxetic behavior [17]. The results indicate that auxetics offer the possibility to improve material properties and optimize the response of components to different load cases. This is one of the assumptions on which this thesis is based and which makes it worthwhile to advance research in the field of auxetics.

Another paper [14] critics that auxetic materials are not sufficiently applied in practice. There is a wide variety of laboratory studies with auxetic materials, however, there are only a few reports of practical application. According to this study, auxetic materials are a great opportunity for many different areas of research. This knowledge gained should not only remain in laboratories but should also be made available to the public to benefit from these novel materials. By continuing research and practical experiments in this field and testing different structures, pure research is to be brought closer to practical application. Besides, some challenges mentioned in the paper such as the substantial porosity of materials with auxetic behavior should be further investigated. The analysis of the bending and compression behavior of different structures will help to understand how the mechanical capability can be optimized.

In addition, a method has been developed to create cementitious cellular composites (CCC). As they cannot be printed directly with the 3D printer yet, they have to be

cast in a mold with auxetic structures. At first a negative mold was printed with a 3D printer. This mold was vacuum impregnated with a silicone rubber to generate reusable molds that are easy to demold. These could be cast and demolded to obtain an auxetic CCC (ACCC) test specimen that can be tested and investigated. Due to non-availability of the instruments, the silicone rubber was not used for this thesis and the method was adapted accordingly. Instead of using silicone molds, the mortar was cast directly into the 3D printed molds. It was also found in the paper that the brittleness and low deformability of CCC in comparison to materials like plastic or textiles make it more difficult to achieve auxetic behavior. Allowing enough deformation inside the structure to enable auxetic behavior, the structure needs an adequate crack bridging ability. This was investigated on an ellipsoid structure with repeating unit cells. Because of the compressive load the quadrangular segments are forced to rotate, forming the shape of a peanut as to be seen in Figure 1. This induces the negative longitudinal strain and the auxetic behavior, respectively.

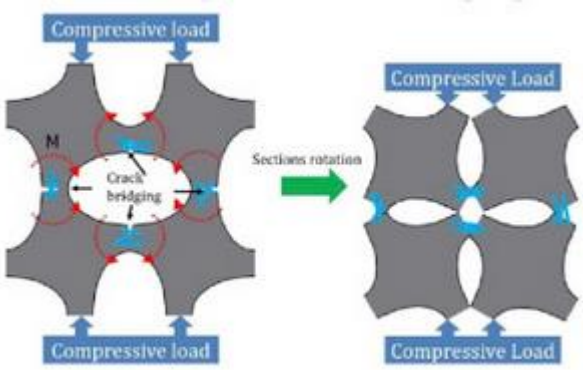

Figure 1: Rotation Leading to Auxetic Behavior [15]

Hence, the joints between the alternate vertical and horizontal oriented ellipses need to bear compressive as well as tensile forces to facilitate the rotation of the structure. As CCC can only carry compressive forces, at least 1% but better 2% of fibers in the mortar mixture are required to bear the tensile forces. For the rotation, small cracks at the edges of the voids are necessary. The results displayed a curve with two peaks, the first symbolized these small cracks while the second showed the actual failure. An adequate crack bridging prevents the immediate failure and thus induces the auxetic behavior of the structure. Four-point-bending, uniaxial compression, and cyclic loading tests on cube and beam specimens, respectively, were performed to confirm the simulation results. The DIC method was used to determine the transverse and the axial strain in order to identify the Poisson's ratio and with it the auxetic behavior. It is pointed out that this study can be used as a basis for future research. Especially the energy dissipation of this auxetic material can be furthered studied as it is very auspicious and can still be enhanced for instance by varying the cellular structure and the constituent material [15]. The findings of this study are to be continued in this thesis. A different mixture for the material will be used, different structures will be printed and compared, and experiments with different load cases will be conducted. For cost reasons, fibers were initially waived for the cubes. Since different structures and a different mixture have been used and there is only one study that has tested the auxetic behavior of CCC, the need for fibers should be re-examined. For the construction industry, it would be easier not to use fibers for the tensile forces as they are not applicable on actual components as on test specimens. Fibers were then used for the beams, as here the tensile forces are also significantly higher.

With the same structure type of alternate ellipses different geometries with different unit cell sizes and ratios between the major and the minor axis of the ellipse were investigated. The results show that an ellipse with both axes equal to 8mm does not show auxetic behavior whereas the geometries with 6x10mm and 4x12mm have a negative Poisson's ratio. Good agreement was found between the experiments and the FE (finite element) simulations. [18] Since auxetic behavior has already been sufficiently studied on ellipsoidal structures, other structures were tested in this thesis. However, three of the four created structures were also varied in size to determine the necessary parameters for auxetic behavior.

In summary, the objective of this thesis is to advance the promising field of research of auxetic materials in order to enable a meaningful application in the practice of the building industry in the future.

.

CHAPTER 3

EXPERIMENTAL METHODOLOGY

The goal of the experimental part of this thesis was to find a structure that induces auxetic behavior in a construction component made of concrete. Since manufacturing of a construction component in original size would be too complex and especially not testable in a usual testing machine, the size is reduced in accordance with the ASTM (American Society for Testing and Materials) standards. Due to this reduction and the auxetic structures inside the sample the use of concrete as the construction material was not suitable anymore because the aggregates inside the concrete are not at scale and would change the actual behavior of the sample. Therefore, mortar is used instead, which has similar properties, but consists only of sand, cement, and water. This material in conjunction with auxetic behavior is referred to as Auxetic Cementitious Cellular Composites, or ACCC. To reach the goal of detecting an auxetic structure for concrete, existing auxetic structures for other materials like steel were considered and evaluated, taking into account that concrete is a very brittle material. Four different structures were chosen. As already mentioned, 3D printing is a great opportunity to create any imaginable structure in a short amount of time. Hence, the idea of an 3D printed mold as formwork for a mortar sample with an auxetic structure was developed.

As concrete is mainly used for components subjected to compression and bending, two series of tests with cubes and beams, respectively, were developed and tested according to ASTM standards in order to see which of the structures behave auxetic and which structure is the most auxetic one.

Technical Requirements

For the experimental part of this thesis a lot of equipment was needed. First of all, AutoCAD was used for creating and designing the molds for the mortar samples with the different structures and preparing them for the 3D print.

To make a 3D model readable and printable for a 3D printer it must be inserted into a slicing software, where the 3D model is sliced into different layers that are supposed to be printed by the 3D printer. In the slicing software the properties of the layers are specified by for example settings about the layer height, the shell thickness, the infill, the printing material, speed, cooling and supports. For this case the slicing software Simplify 3D and Cura were used depending on which 3D printer was operated.

Due to a large number of samples three different 3D printers were used: The Maker Gear M3 ID, the Creality CR-10 and the Creality CR-6 SE. Whereas the Maker Gear M3 ID has a dual extrusion which means that it can print with two nozzles at the same time, the two Creality printers have only one nozzle.

After an evaluation and testing of different filament types polylactic acid (PLA) was used as the printing material because of its good characteristics such as printing simplicity and not too much flexibility. The mortar mixture will be presented later in this chapter.

The experimental setup for the compression tests consisted of the AGS-X 100kN Shimadzu machine with Trapezium as a controlling software, a tripod, and a phone camera of a OnePlus7t as to be seen in Figure 2. In order to assess whether auxetic behavior has occurred, the displacements must be recorded and determined during the test. The Digital Image Correlation (DIC) method was used to determine these displacements. For this method a camera is used to record the experiment and an open-source software called Ncorr tracks changes in the images afterwards so that the displacements can be determined. For the three-point bending tests, the BFS-U3-50S5M-C USB 3.1 Blackfly S, Monochrome Camera specially manufactured for the DIC method is used, which immediately converts the video into separate monochrome images. The camera shoots 35 frames per second with a resolution of 5 megapixels. The sensor format is 2/3”.

Figure 2: Experimental Setup

Structures

As already mentioned, there are plenty of already existing auxetic structures. However, most of these are used for ductile materials like steel. This comes from the fact that a basic requirement for auxetic behavior is that the structure contracts under compression until it is a compact structure and behaves like a conventional material again. For this purpose, the material must be able to deform before it breaks. The problem with concrete, being a brittle material is that it breaks immediately without any warning and has a very low deformability. Therefore, the goal for designing the structures for the mortar molds was to find a balance between enough voids to enable deformation and auxetic behavior, and enough solid material to prevent the concrete from breaking immediately, thus increasing the timespan where deformations can happen. This is also the reason why three of the four different kinds of molds have two versions so that a perfect void ratio can be determined.

As long as there are no existing auxetic structures for concrete besides of ellipses [15] and diamonds [13], auxetic structures for other materials were taken as a base and their thickness was increased so that auxetic behavior of the mortar sample could be achieved. Figure 3 shows how the thickness of the original structure was increased and then converted into a structure for a mortar mold in the shape of a cube or a beam, respectively.

Figure 3: Structure Design (Resource: [19])

The original structures were the following:

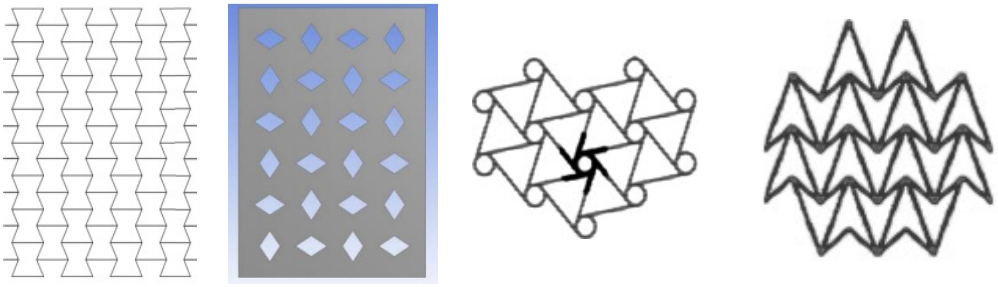

Figure 4: Original Structures (Resource: [13, 19, 20]

By increasing the thickness of the original structures, the following seven different mortar molds for the compression test could be developed. The molds are illustrated in Figure 5-11. The figures each show a printed mold and the AutoCAD model with appropriate dimensioning. As already mentioned, there are only four different kinds of molds based on the original structures but three of them have two different versions. Owing to the fact that auxetic behavior of mortar or concrete is still in its infancy, the perfect void ratio or the ratio of the size of the structure to the size of the gaps between the structures has not been identified yet. Hence, different versions were developed to learn more about the basic requirements for achieving auxetic behavior in a mortar

structure. According to the Standard Test Method for Compressive Strength of Hydraulic Cement Mortars the cube samples are supposed to be a 50mm-by-50mm-by-50mm [21]. Four test specimens of each structure type for the compression tests were created to make the results reliable. The printing of the molds took only about 5-10 hours each. The Standard Test Method for Flexural Strength of Concrete [22] applies to the three-point bending test of concrete beams and implies that the effective span length of the beam is four times the width of the beam. For simplification purposes the width and height of the beams are the same as for the cubes so that the size of the structures can be transferred. Consequently, the beams have a dimension of 50mm-by-50mm-by-225mm with an overlap of 12.5mm on either side. For the bending tests only three test specimens of each structure type were created because three are enough to make the results reliable and the printing of the beam molds took about one day each so that three was just more time-effective than four. The samples of the same Mold type are numbered from 1 to 3 or 4, respectively. For the compression as well as the three-point-bending tests samples without voids were created as a verification of the results.

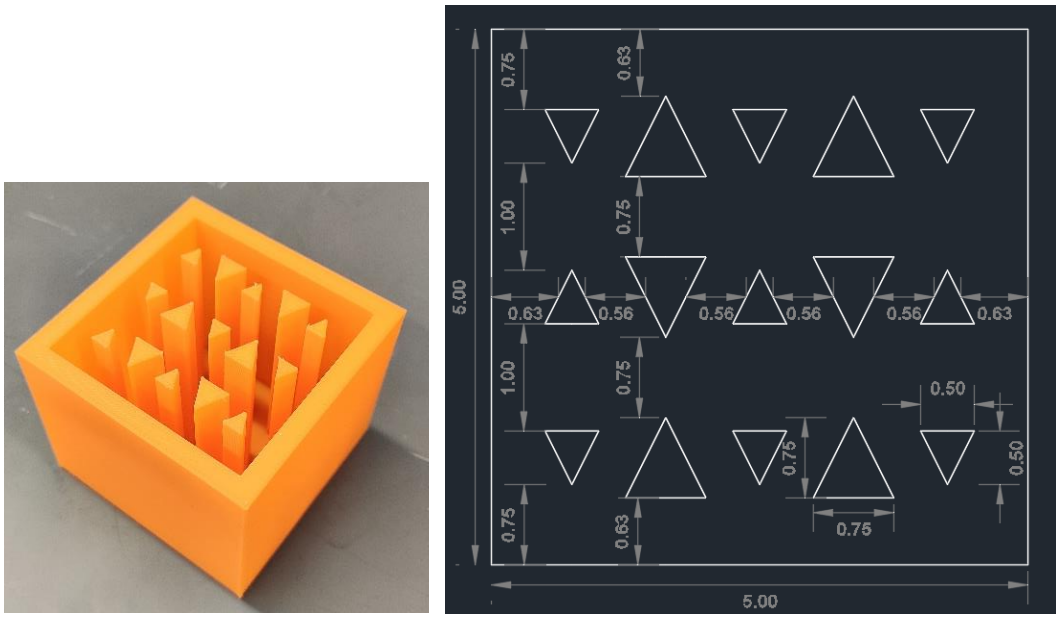

Figure 5: Mold 1 - 3 Rows (Mold 1 – 3)

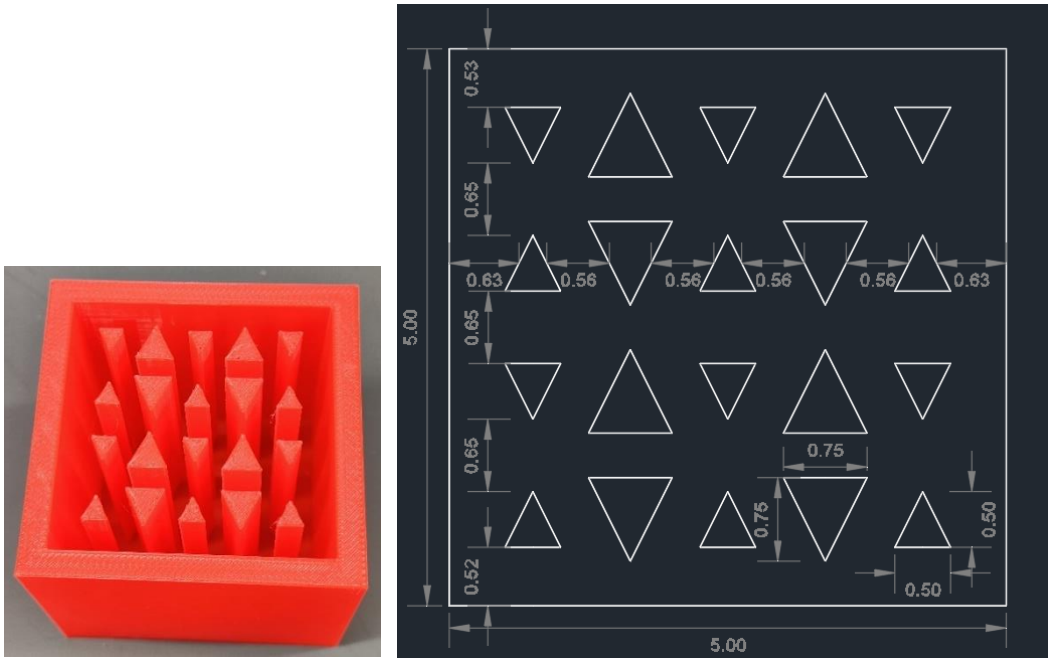

Figure 6: Mold 1 - 4 Rows (Mold 1 – 4)

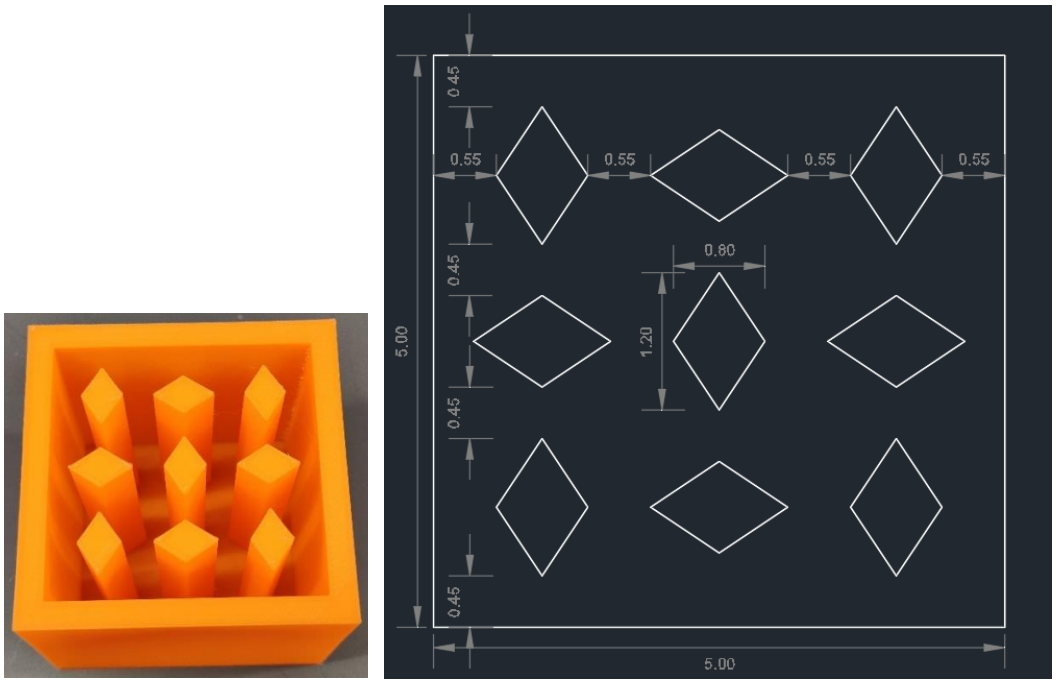

Figure 7: Mold 2

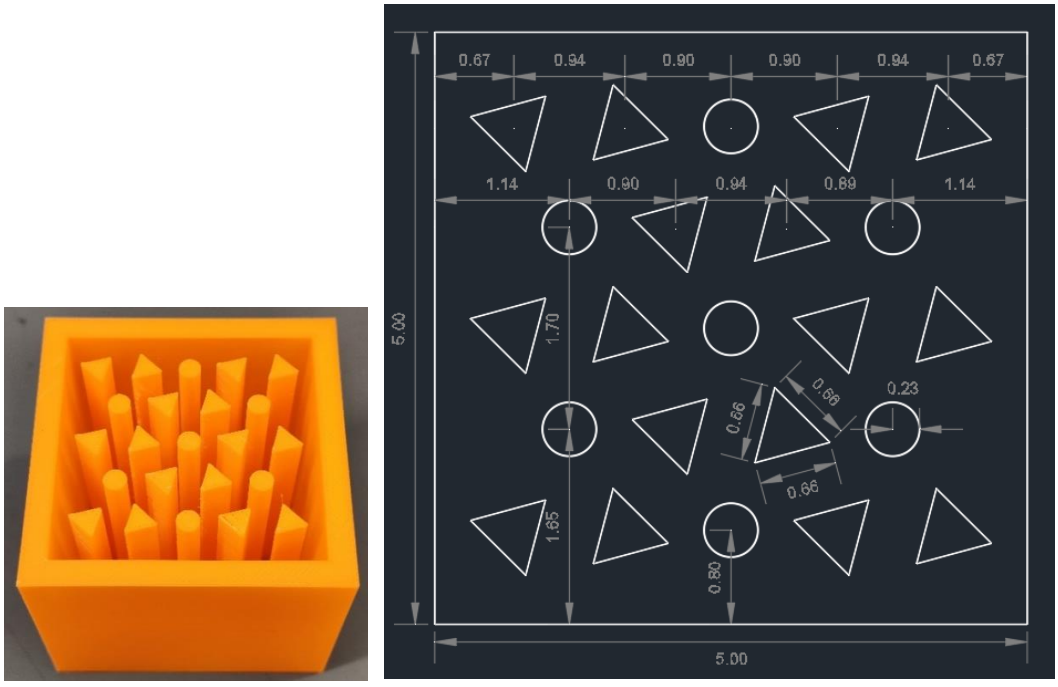

Figure 8: Mold 3 – bigger (Mold 3 – b)

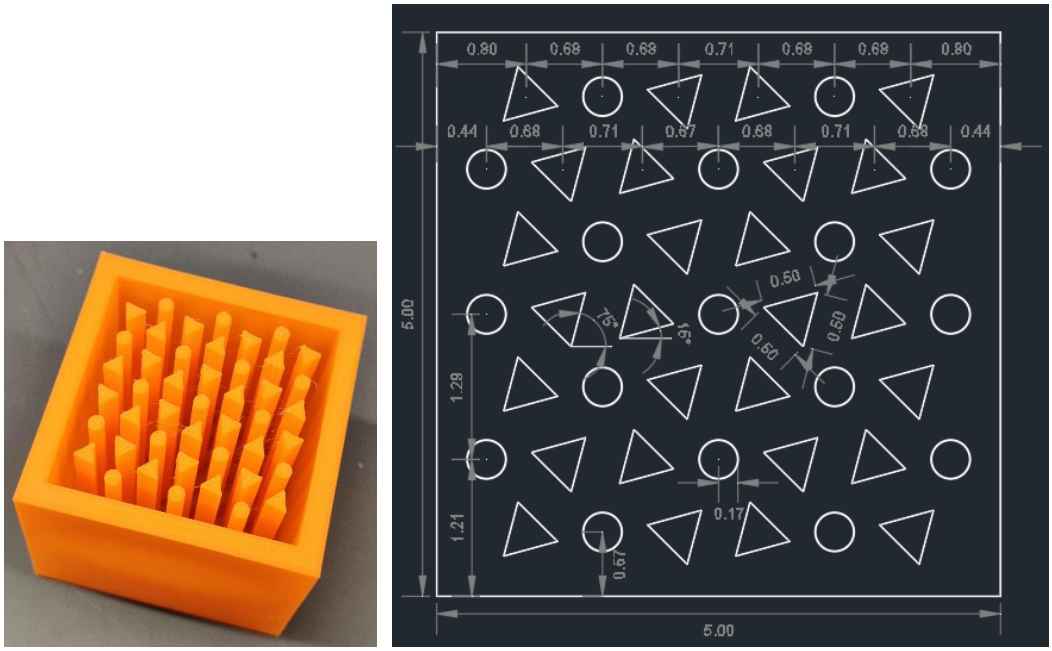

Figure 9: Mold 3 – smaller (Mold 3 – s)

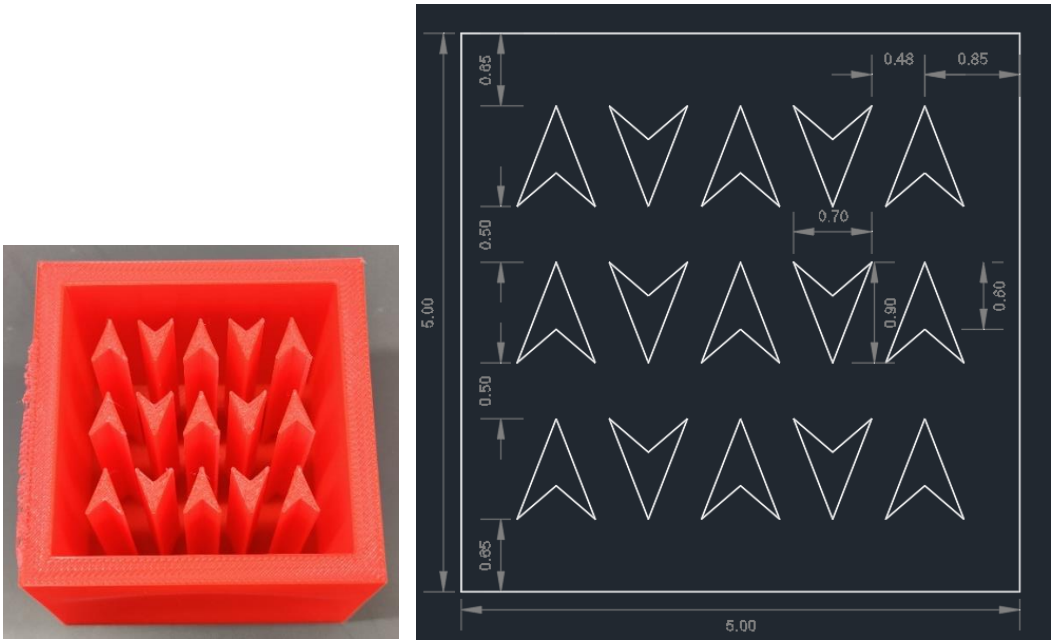

Figure 10: Mold 4 – bigger (Mold 4 – b)

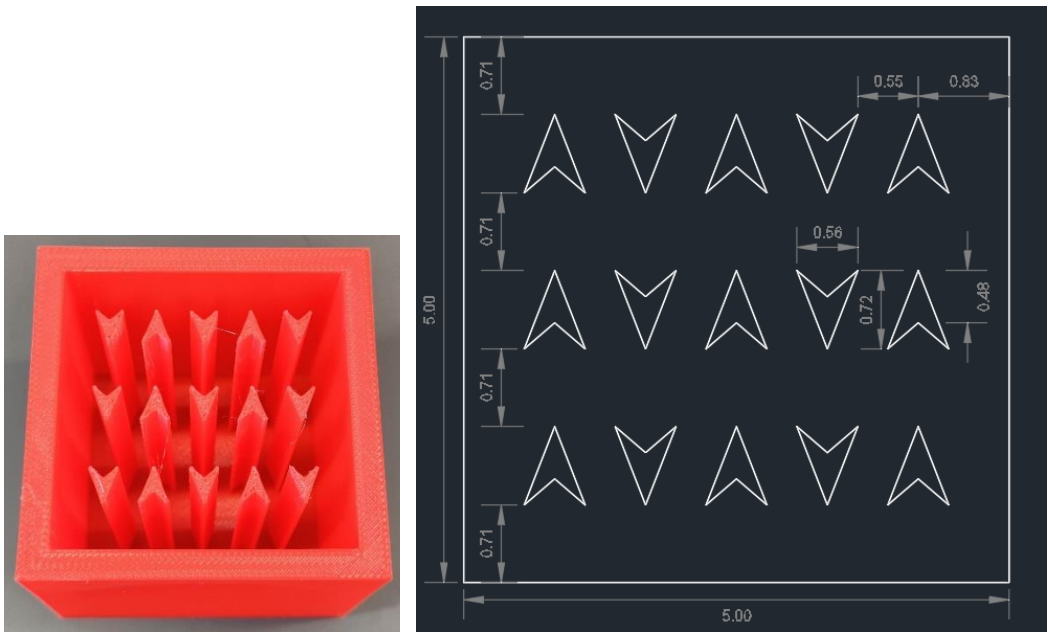

Figure 11: Mold 4 – smaller (Mold 4 – s)

As the goal of these experiments is not only to find the Poisson's ratio and determine if the structure makes the mortar behave auxetic or not but also to determine the compressive strength and flexural strength, respectively, of each structure, the void ratio of each structure was calculated as shown in Table 1. For an actual application in practice a good balance between the strength and the auxetic behavior of a structure is essential.

Table 1: Void Ratio for Cubes and Beams with Different Structures

	Cubes	Beams
Mold – normal	0%	0%
Mold 1 – 3 Rows	11.25%	13.33%
Mold 1 – 4 Rows	15.00%	17.78%
Mold 2	17.28%	17.92%
Mold 3 – bigger	18.17%	20.20%
Mold 3 – smaller	16.48%	18.70%
Mold 4 – bigger	12.60%	14.56%
Mold 4 – smaller	8.06%	9.32%

Printing

PLA was used as filament material for printing. This is due to the fact that the other common filament type TPU (thermoplastic polyurethane) is much more flexible than PLA. That results in buckled walls of the cube, a tough demolding since it's not breakable or sliceable and a high difficulty during printing because especially very small structures in the mold wobble during printing and are not precisely printed anymore. After printing many test samples, the following properties for the molds were selected. The thickness of the walls was chosen to 5mm to make the mold more stable. To decrease the printing time and facilitate the demolding, the infill was chosen to 0% and the shell of the cubes restricted to only one layer. Because of cooling problems, the sides of the cubes started buckling when they consisted of only one layer. Since more layers

made it much harder to demold the cube and the slightly arched sides could be straightened by grinding, the cubes were printed with only one layer. Furthermore, more layers for the shell would also mean more layers for the structures inside the cube. PLA is much weaker than concrete and should not have a big influence on the experiments. However, as most of the structures could not be removed and stayed inside the specimens during testing, the number of layers should be chosen as small as possible to test the actual reaction of the mortar, avoiding any interaction with PLA. Since these experiments are a model-based test for a practical application of auxetic compression and bending elements in the future, the properties of the specimens should be as comparable as possible to beams and compression elements in a big scale. Assuming that these construction elements will not contain any PLA structures, it is also better to choose the number of layers as small as possible.

In beams, however, their side being much longer than in cubes, arching occurred to a greater extent which was not acceptable anymore. Also, it was easier to demold the beams with two layers than the cubes because the sides of the cubes are so short that the mold becomes very inflexible which is good for the experiments but difficult to demold. Hence, the shell of the beams was printed with two layers. The bottom must be more stable in order to prevent damage during casting and is also easier to demold in one piece if it has four to five printing layers. The layer height was chosen to 0.2mm as a compromise between printing time and accuracy. In addition, it was observed that transparent filament is easier to demold than other colors.

Mortar Mixture

After creating the molds as a formwork for the mortar mix the next step was to find the right mortar mixture. As already mentioned, the mortar mix only consists of sand, cement, and water in contrast to concrete where also aggregates are added. The most important characteristics of a suitable mortar mixture are a high compressive strength and a good workability. With increasing water/cement ratio the compressive strength decreases and the workability increases. The molds are fragile and the gaps between the structures are small, so the water/cement ratio needs to be high enough to enable a good flowability. On the other hand, a high compressive strength is needed so that the sample has some time to deform with an auxetic behavior under compression before it breaks. Under these circumstances and after a lot of test mixtures and specimens a water/cement ratio of 0.45 by mass was chosen. Furthermore, the mixture consists of 50% paste which includes water and cement and 50% sand by volume. The cement used is Portland cement type 2 and the sand is Quikrete fine sand.

The following table shows the mixture of the mortar for the compression tests in percent by mass. After calculating the mass for every ingredient around 20% should be added because of measuring inaccuracy and losses and leftovers during mixing. The total mass for one cube is 212g.

Table 2: Mortar Mixture for Compression Tests

Cement ($2.8 g/cm^3$)	Sand ($1.6 g/cm^3$)	Water ($1 g/cm^3$)
36.48%	47.11%	16.41%

The following picture shows the consistency of the mix:

Figure 12: Mortar Mix for Cubes

To remember, concrete is a brittle material and cannot take up tensile forces. Even though the cubes were loaded under compression there will be areas in the cube where tensile forces inside the mortar occur because of the auxetic structures that initialize deformations as described earlier. Such tensile forces are much higher during a bending test in comparison to a compression test. Furthermore, a research group from the TU Delft [15] could only achieve auxetic behavior in mortar when there were also fibers included, which take up the tensile forces. In the present thesis, actual reinforcement was not usable for a sample with small structures inside, therefore fibers were added to the mortar mix for the three-point bending tests. The fibers greatly increased the viscosity of the mortar mix. That's why a few drops of superplasticizer were added to the mix. The amount of superplasticizer was according to the amount used in the paper [15]. Superplasticizer increases the workability without decreasing the compressive strength as a higher water/cement ratio would do it.

For identifying the perfect volume of fibers three test mixes with 0.5%, 1% and 2% of fibers by volume were produced. The goal was to use as much fibers as possible while maintaining good mortar flowability and ensuring homogeneous fiber distribution. For the mix with 2% of fibers this was not possible anymore as the fibers could hardly be pushed into the molds in the gaps between the structures. The mixes with 0.5% and 1% were both still workable so the mix with 1% of fibers by volume was used. The fibers were PVA fibers with a length of 0.5in. Table 3 shows the mixture of the mortar for the three-point bending tests in percent by mass. Again around 20% for every ingredient should be added to supply a reserve for losses during the casting process. The total mass for one beam is 1142g.

Table 3: Mortar Mixture for Three-Point Bending Test

Cement ($2.8g/cm^3$)	Sand ($1.6g/cm^3$)	Water ($1g/cm^3$)	Fibers ($1.28g/cm^3$)	Superplasticizer
36.05%	46.81%	16.38%	0.76%	0.05083%

The following picture shows the consistency of the mix:

Figure 13: Mortar Mix for Beams

Casting and Demolding

Cement and sand were mixed first until they were equally distributed. Then the water was added and stirred with a shovel until it was a uniform mix without any dry cement-sand chunks. The molds were sprayed with WD40 before they were filled to make the shell more slippery and thereby facilitate the demolding. During pouring into the mold the mortar mix usually sticked at the top parts of the structure especially for the molds with very small gaps. Manually shaking was difficult because of the brittleness of the molds. Therefore, a vibration table was used to shake the mortar into the mold equally distributed between the structures. As the cement gets separated from the water when the mortar is vibrated too long, the vibration table should only be used for a few seconds so that the mortar can slide between the structures. For the beams shaking the mortar mixture between the structures did not work very well because of the fibers. Even if the mortar still slipped into the mold the fibers would be stuck at the top of the structures. Therefore, a small object like the back end of a plastic spoon was used to push the fibers between the structures and make them distribute uniformly without sticking together and letting them separate from the mortar. When the mold was full of mortar the vibration table could be used for another 30 seconds until all or at least most of the air voids inside the mortar mix especially along the structures could escape in form of air bubbles. Since the mix dries out with time not more than ten cubes should be cast at the same time.

After the casting the cubes were stored for around 48 hours on a flat surface under a plastic wrap so that the mortar could cure before it got demolded. During curing the mortar produces heat which makes the water evaporate. If too much water evaporates

the mortar dries out and forms cracks. The plastic wrap collects the water so that the cube is still in a moist environment and cannot dry out.

For demolding pincers and a slotted screwdriver were used for removing the walls of the cube and a spattle for removing the bottom. Sometimes it was difficult to remove the bottom layers but the PLA got brittle after 28 days so it could get removed then or in the worst case it had to be ground away. It was also tried to heat up the cube to about 60°C to make the PLA soft again so that it is easier removable. After three hours no difference in the consistency of the PLA could be determined and the temperature could not be increased any further because that would dry out the mortar, so this method was discarded.

After demolding the cubes were kept in a water bath for at least 28 days. Citric acid can be added to the water to accelerate the curing. It was ensured that the entire cube was under water to prevent dehydration.

Testing

DIC Method

Digital Image Correlation is an innovative technique to measure strain and surface displacement on every material. It is a non-contact optical method, that is cost-effective, accurate and simple to use. It basically compares all the images taken during an experiment with the reference image and determines the deformation from the changes in the pictures. This works by forming a grid of unique pixel blocks on the surface and tracking their deformation during the experiment. For this a random pattern of black dots on a white surface of the test specimen is needed so that around half of the surface area is painted black and the other half is white. [23] Also, the dots should be uniform in size,

around 3-by-3 to 7-by-7 pixels big, and fully adhered to the sample, so that the deformation of the sample corresponds to the deformation of the pattern [24].

Thus, the first step was to dye the test specimen with white paint and black dots. Different methods were considered. The first was to just paint a random pattern of black dots by hand with an ultra-fine permanent marker. For this technique the white paint Semi-Gloss Protective Enamel – Superior Coverage & Durability by Rust-Oleum was used to dye the specimen white. Since this method was the most accurate and easiest one without a lot of needed equipment it was used for painting the cubes. The following picture shows how accurate the painted cubes look like.

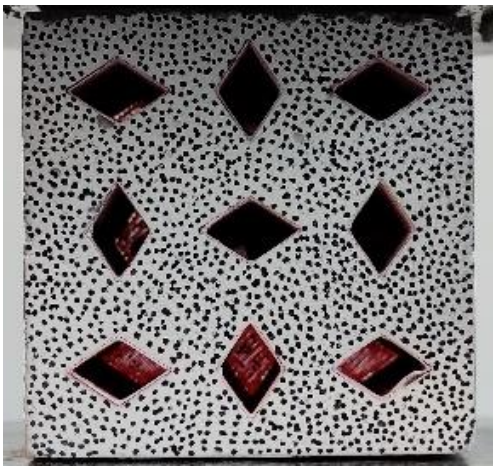

Figure 14: DIC-Method pen

As the cubes were small (25cm² less the voids) it took like 20min to paint every cube which is time-intense but still possible. For the beams in contrast, it would have taken 32 hours which is mis proportioned. Therefore, other methods were considered.

It was tried to just spray with spray paint on the specimen or use a toothbrush or any other kind of brush, spraying black paint on the bristles of the brush and sprinkle the black paint onto the white painted test specimen. Since the test specimens were still

small and had structures inside and the dots had to be small enough so that the DIC software is still able to distinguish the black holes of the structures from the black dots of the pattern, this method was not applicable. The sprinkles were too big, and it was too difficult to distribute the black paint uniformly on the entire specimen as to be seen on the following picture.

Figure 15: DIC-Method spraying

Another idea was to print a paint roller with the 3D printer. A speckle generator software created a random pattern of black dots. This pattern was transferred to a designing software like AutoCAD where the dots were converted into bumps on the paint roller. The following picture shows the printed paint roller.

Figure 16: Paint roller

After printing, the paint roller was rolled over the white painted specimen, but the dots were too rare, undefined and the paint did not really stick to the surface of the

sample as to be seen on the following picture so that the DIC software would have lost correlation.

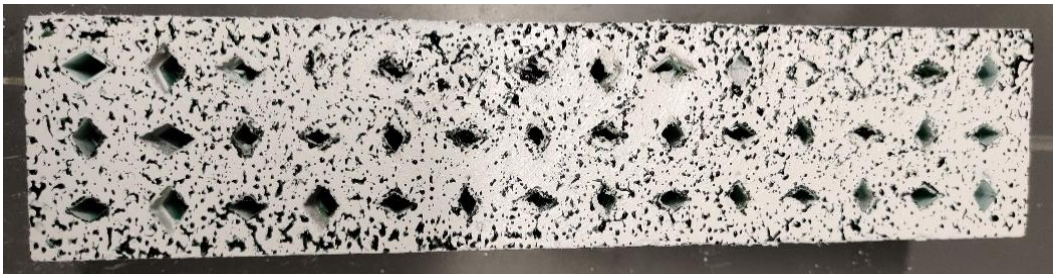

Figure 17: DIC-Method paint roller

The next considered method was hydro dipping. This procedure can be used for printing any possible picture on a three-dimensional object and can be applied on almost every surface. The test specimen was painted white as a base coat with the paint that was used before. This base coat should make the film stick to the specimen. A normal ink printer was used to print the black dots onto a water-soluble film. This film was sprayed with an activator to dispense the ink from the film and placed on the water surface of a water filled container that is big enough to fully submerge the test specimen for around one minute. One side of the film is supposed to absorb the water to hydrate the film. This side should face down. Then the Hydrovator Hydro-Printing Activator by Southern Hydrographics was used to make the film dissolve. When it was fully dissolved the sample was pushed into the ink on the water in a 45-degree angle. The slimy residue was rinsed off afterwards. Unfortunately, the dots were too big because they got increased through the water. Also, after rinsing it looked like there would be a water film on the specimen that made everything flow apart and made the specimen unusable

for the DIC method. The following picture shows two beams painted with the hydro dipping method.

Figure 18: DIC-Method hydro dipping

The last method that finally worked for the beams was using a handheld printer. The printer that was used was the MBrush Portable Mobile Color Printer by Kongten. The pattern of black dots was generated with the speckle generator and a screenshot of the pdf could be entered from a phone into the app that controls the printer. A few settings like the size of the pattern, the density, brightness, and saturation could be made. As the printer can only print a picture with a height of 1.429cm the picture that was chosen in the app to be printed could be sliced so that the printer would print slice after slice of the picture. Reprinting the same slice again would be unusable for the DIC software as it would lose correlation because of repeating patterns. The printer worked very well on the paper but on the concrete sample with the white paint that was used before, the black dots faded with time and were not visible enough for the DIC software. Very fine sandpaper was tried first but that increased the size of the black dots so that the pattern was not applicable anymore. Flat white paint from Rustoleum (Ultracover paint

+ primer) was used. The ink sticked much better on this paint and finally a method to paint the black dots on the test specimens was found (Figure 19). As the black dots still faded after some hours the experiments should be performed right after printing.

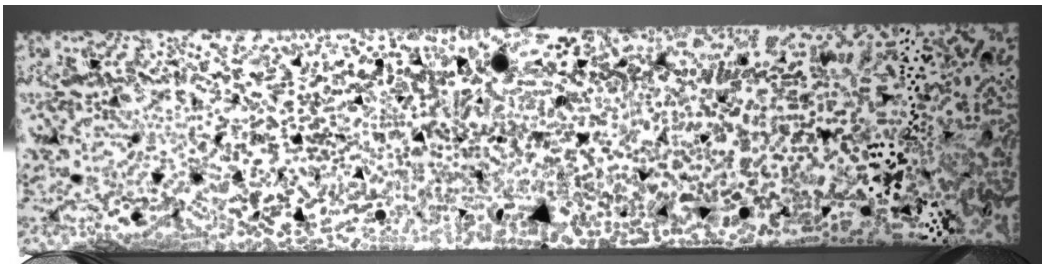

Figure 19: DIC-Method handheld printer

The next step was to get the pictures that had to be analyzed into the DIC software. A phone camera of a OnePlus 7t with 60fps and 4K was used to film the compression tests. For the three-point-bending tests a DIC camera with 35fps and five megapixels was used. The advantage of this camera was that the recording could be controlled with a software on the computer that also controlled the testing machine. Also, the camera takes monochrome pictures instead of a color video so that the step of converting the video into pictures can be skipped. To reduce the number of pictures taken during the experiment the DIC software was set at four pictures per second. The phone camera or the DIC camera had to be placed on a stable tripod that did not shake during filming and positioned normal and central to the surface to be examined for deformations. At first a picture with a ruler or some other kind of reference had to be taken as a calibration image so that the right scale for the deformations could be set later in the DIC software. Then the experiment and the filming should be started simultaneously so that the time of the experiment and the time of the captured pictures match for the analysis.

For converting the video from the phone camera into pictures, the software Free Video to JPG Converter was used and one picture per second was converted. The open-source software Ncorr that was used for the DIC analysis could only analyze around 130 pictures at the same time. So, it had to be guaranteed that the number of total pictures did not exceed this number.

Another problem was that the name of the pictures that are proceeded by the DIC software had to have the format name_#.tiff. This was not the case for the phone camera pictures as well as the DIC camera pictures. The software Bulk Rename Utility was used to change the name of the pictures into a format that fits for the DIC software.

Then finally Ncorr could be started to analyze the displacements. Ncorr is a software that is running on the platform MATLAB and requires the Statistics and Machine Learning Toolbox and the Image Processing Toolbox. The first step after installing Ncorr was to insert the reference image which is the first image of the section that is to be analyzed. For just determining if the sample shows auxetic behavior or not, the linear part before the first crack was taken. In this part of the curve the specimen is already loaded, should not move anymore and just deform according to the load. In this section auxetic behavior should be visible if it happened. For determining the Poisson's ratio, the section between the start of the loading and the first crack would have to be taken. The pictures of this section including the reference picture had to be added to the software next. For this step two different options are offered, Load All (memory heavy) or Load Lazy (slower but less memory). As the analysis takes a long time anyway the memory heavy option is recommended especially for bigger specimens. The next step is to set the region of interest. The drawing option of a rectangle was chosen. Important

is that the region of interest is not supposed to cover the entire specimen area because the DIC software would lose correlation if the test specimen moved out of the region of interest during the experiment because of deformations. The region of interest must therefore only be so big that the edge of the test specimen remains outside the edge of the region of interest during the test. For determining the Poisson's ratio, the edge of the region of interest should be as close to the edge of the test specimen as possible. To be able to see only the tendency of the auxetic behavior, it does not have to be quite that big.

Then the DIC parameters had to be set. The subset radius which defines the size of the subset included around nine black dots to get the best analysis results. The subset radius which defines the size of the pixel blocks should be set so that the pixel blocks are about as large as the space between the black dots. The last step before the analysis is to allocate the subareas of the test specimen to the seeds of the processor of the computer that is used for the DIC software. The subareas should all be of the same size in order to perform the analysis as quickly as possible. After the analysis the right scale for the deformations had to be set. Therefore, in the Format Displacements section, the calibration image that was taken before the experiment has to be uploaded. Then usually a length of 10mm had to be marked in the image to scale the deformations from the picture size to the actual size of the specimen. Then the displacement could be plotted picture by picture and the displacement and the behavior during testing could be read off.

Compression

The compression experiments were performed according to the Standard Test Method for Compressive Strength of Hydraulic Cement Mortars [21]. The experiment enables determining the compressive strength of each auxetic structure. Because mortar should be cured for 28 days it does not really matter if the cubes are tested after exactly 28 days or later [25]. For this case the cubes were taken off the water bath after around 30 days. As painting them white was needed for the DIC analysis they were painted after taking them off the water bath and the paint had to dry for another two days. Because of casting the cubes in the 3D printed molds, the walls were not perfectly straight. As already mentioned, the molds were printed with only one layer so that the walls buckled out a little bit. To distribute the pressure of the compression machine uniformly on the whole area of the cube, the cubes had to be ground before they were tested. They were ground with an angle grinder.

The testing machine consists of a fixed round steel plate with a diameter of 10cm where the cube sits on and a same sized steel plate over the cube that moves downwards to compress the cube. As auxetic behavior can only occur when the cube is loaded orthogonal to the auxetic structures, the test specimen had to be placed between the plates so that the white painted side that shows the auxetic structure is in the front and parallel to the machine and the camera. The top plate was moved as far down as possible without touching the test specimen and putting a pressure on it. The setup is to be seen in the picture below.

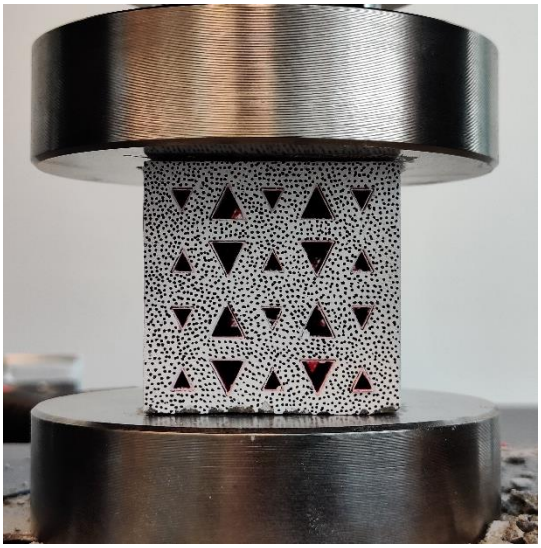

Figure 20: Setup for Compression Test

Then the experiment could be started in the Trapezium software on the computer that was connected to the testing machine. To facilitate a static loading the loading rate was chosen to 1mm/min.

The experimental results that can be exported as a CSV file from the machine controlling software are time, force, and stroke. The file had to be converted into excel so that the stress-strain-curve can be calculated.

$$Stress\ \sigma = \frac{Force}{Area} = \frac{Force}{50 \times 50}\ \left[\frac{N}{mm^2}\right]$$

$$Strain\ \varepsilon = \frac{Stroke}{Height} = \frac{Stroke}{50}\ \left[\frac{mm}{mm}\right]$$

As the timespan between starting the experiment and loading the test cube is different for every test specimen but does not tell anything about the behavior of the cube under compression, the point in time where the actual loading of the specimen started had to be zeroed so that the stress-strain curves and especially the young's modulus are

comparable. The charts were generated in Grapher. In order to create a demonstrative comparison basis for the different molds, a plot was created with the stress-strain curves of all molds together. For this purpose, the results of each mold type were averaged and combined to form one curve. As the tests were stopped at different times, jumps occurred in the originally averaged curve. Therefore, a trendline was created with the function Fit Curve and the Fit Type LOESS in Grapher. LOESS stands for locally estimated scatterplot smoothing [26].

Bending

The three-point-bending experiments were performed according to the Standard Test Method for Flexural Strength of Concrete (Using Simple Beam with Third-Point Loading) [22]. As already mentioned, the effective span length of the beam has to be four times the width of the beam. Since the width of the beam is 50mm the effective span length has to be 200mm. The beam is located centrally on two supports. The supports are cylinders with a diameter of 3cm orthogonal to the beam so that they are not districted during the bending experiment. The third point is the point in the middle of the beam that pushes the beam uniformly over the whole width down. As the determination of a good DIC method for the beam experiments took a long time, the beams were taken off the water bath around 50 days after molding. Since the beams were more uniform than the cubes because of two printing layers of the shell and furthermore the beams were only supported at 3 points and not bearing on an entire side, grinding was not necessary. Similar to the cubes, the beams were loaded orthogonal to the structures so that the side with the structures could be filmed for the DIC analysis. The setup is to be seen in the picture below.

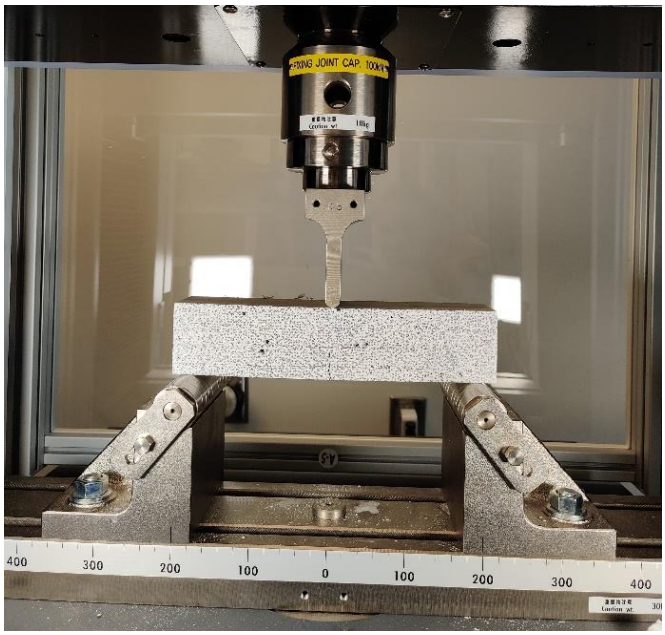

Figure 21: Setup for Three-Point-Bending Test

Then the experiment could be started through the controlling software Trapezium from the connected computer. The static loading rate for the three-point-bending experiments was 0.375mm/min.

The experimental results that can be exported as a CSV file from the machine controlling software are time, force, and stroke. To generate a force-displacement chart for every structure type the CSV file had to be converted into an excel file. For simplification the stroke that is measured at the top edge of the beam is assumed to equal the displacement that is usually measured at the centerline. For the comparison of the different structure types two charts were generated that show the averaged curves of the eight structures. One chart shows the relationship between force and displacement and the other one the relationship between flexural strength and displacement. The flexural strength is calculated by:

$$Flexural\ Strength\ \sigma = \frac{3FL}{2bd^2} = \frac{3 \times 200 \times F}{2 \times 50 \times 50^2} = 0.0024F\ \left[\frac{N}{mm^2}\right]$$

The point in time where the actual loading of the specimen started had to be zeroed again so that the curves are comparable. The charts were generated in Grapher. As for the results of the compression experiments, a plot was created with the stress-strain curves of all molds together to facilitate the comparison of the different structure types. For this purpose, the results of each mold type were averaged and combined to form one curve. As the tests were stopped at different times, jumps occurred in the originally averaged curve. Therefore, a trendline was created with the function Fit Curve and the Fit Type LOESS in Grapher. LOESS stands for locally estimated scatterplot smoothing [26]. As the flexural strength is an important characteristic of bending elements, one chart with the flexural strength-displacement for all molds is created. The procedure to obtain the averaged curves is the same as just explained for the force-displacement chart.

.

CHAPTER 4

RESULTS

This chapter deals with the description and evaluation of the results of the compression and three-point-bending tests. The compressive and flexural strength are discussed and differences between the different types of molds are determined. The description of the types of molds can be found in the chapter “Structures”. In addition, it is amplified how the auxetic behavior can be identified with the help of the DIC method. Thus, all test specimens are examined, analyzed, and compared for auxetic behavior. Furthermore, challenges and uncertainties are pointed out, which leaves opportunities for future work open.

Compression Tests

For the compression tests four test specimens for each mold were printed, cast, demolded, painted, tested, and analyzed. As the fourth mold of Mold 2 broke during casting, there are only three molds investigated. The data is determined, and the plots are compiled as described in the Compression Test section.

Compressive Strength

As to be seen in Figure 22 the test specimens all show very different compression behavior. Figure 22(a) shows the stress-strain curve of the normal molds without any auxetic structure. Mold_normal_1 and Mold_normal_4 have a very similar behavior with a maximum stress of around 40MPa and a strain of 3%. These two specimens also failed right after they reached their maximum compressive strength without any advance notice. Mold_normal_2 had a pre-crack, but the stress has still increased after that. All

four molds had a similar young's modulus of around 1800MPa. Figure 22(b) shows how different the results of actual experiments in comparison to the theory of compression tests can be. Even though the young's modulus seems to be similar for all four molds, they all cracked at completely different stress levels that vary from 2MPa to 17MPa. Although two of the Mold 1 test specimens with 4 Rows in Figure 22(c) had probably a pre-crack they all could reach a similar stress level. Mold 2 in Figure 22(d) is definitely the mold where the results of the test specimen resemble each other the most. For all of them the young's modulus is around 1000MPa, the stress varies from 4 to 5 MPa and the strain is around 0.7%. In contrast to Figure 22(e) and Figure 22(g) where the young's modulus is similar but the stress and strain level at failure vary a lot, Figure 22(h) shows a very similar behavior between three of the four test specimens. For this Mold 4-smaller the maximum stress is around 13MPa and the strain at failure around 1.3%. The compression behavior of Mold 3-smaller in Figure 22(f) shows a similar young's modulus and a similar maximum strain level for three of four molds of around 1%. The compressive stress at failure varies from 2.5 to 7.5MPa.

This very diverse behavior probably comes from the fact that the sides of the cubes were not perfectly flat. As they were cast in 3D printed molds with shells with only one layer, the sides were a little bit convex or concave, respectively. Even though they were ground in order to make the surfaces rectangular and straight, it was only by visual judgment. For the compression test a tenth part of a millimeter is enough to load the cube unequally and cause a stress concentration at one point that leads to a crack. While concave surfaces induce a higher pressure at the edges of the cube, convex surfaces

provoke a higher compressive stress in the middle of the cube. This leads to very different fracture behavior and could explain why the young's modulus for each mold type is similar for most of the molds, but the moment of failure differs greatly. In order to avoid this bulge of the cube sides in the future, either silicone rubber molds should be used as in the paper [15] or a better method to demold 3D printed molds with more than one layer has to be developed.

Another problem might be the sharp edges of some of the srcutures. Since the stress concentration is much higher at sharp edges than at round edges this could also lead to a faster and more immediate failure. Together with a slower loading rate, rounded edges could give time to the test specimen to deform and carry more load.

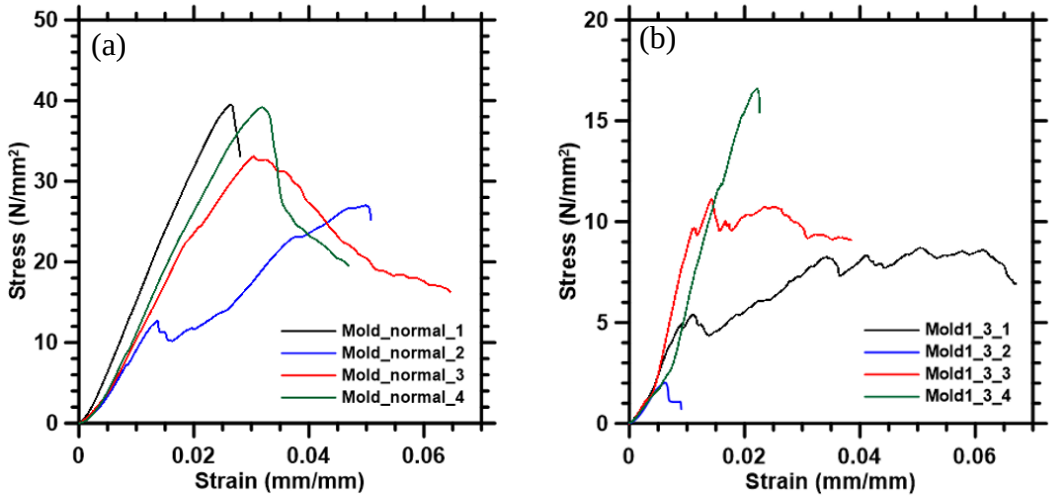

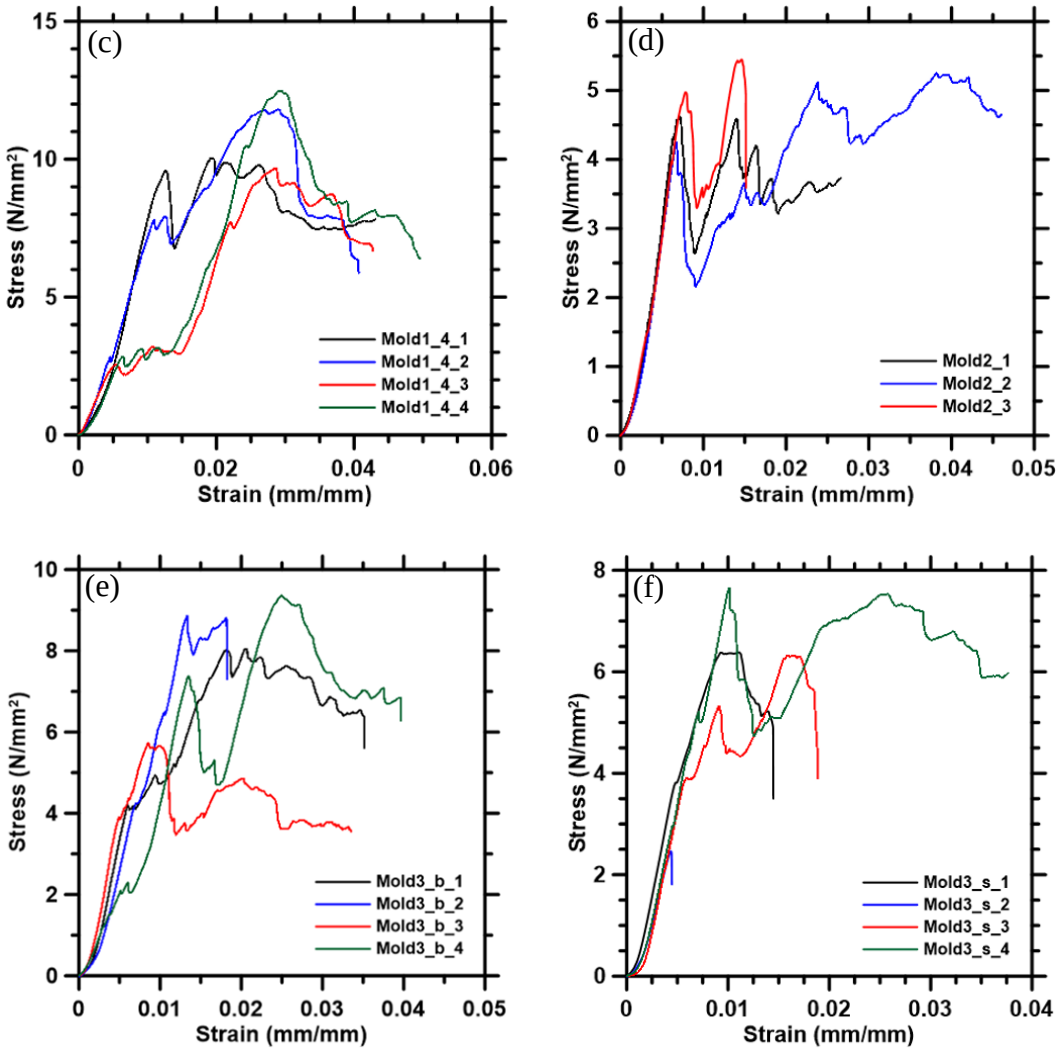
(c)
Stress (N/mm²)
Strain (mm/mm)
Mold1_4_1
Mold1_4_2
Mold1_4_3
Mold1_4_4
(d)
Stress (N/mm²)
Strain (mm/mm)
Mold2_1
Mold2_2
Mold2_3
(e)
Stress (N/mm²)
Strain (mm/mm)
Mold3_b_1
Mold3_b_2
Mold3_b_3
Mold3_b_4
(f)
Stress (N/mm²)
Strain (mm/mm)
Mold3_s_1
Mold3_s_2
Mold3_s_3
Mold3_s_4

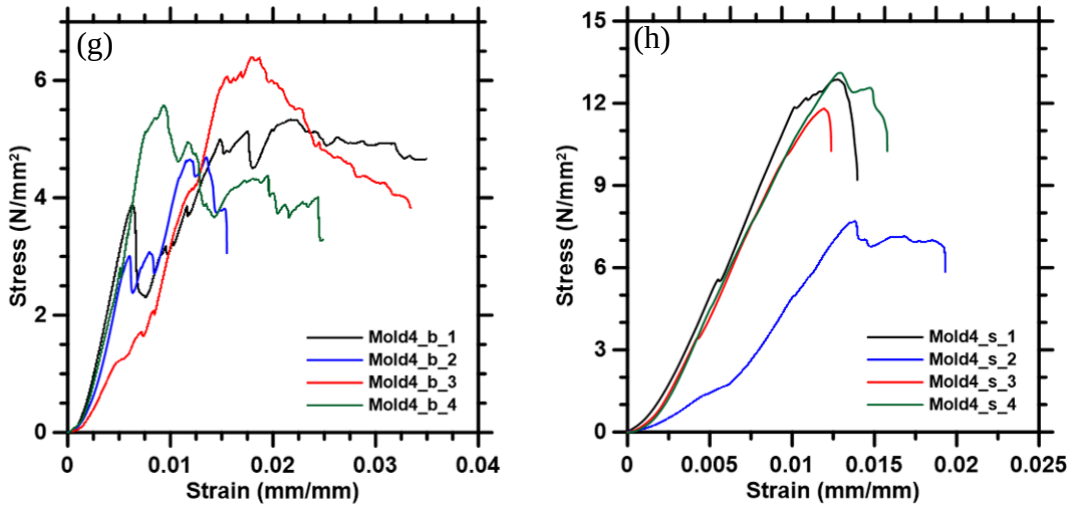

Figure 22: Stress-Strain Curves for Compression Tests for (a)Mold normal, (b)Mold 1-3Rows, (c)Mold 1-4Rows, (d)Mold 2, (e)Mold 3-bigger, (f)Mold 3-smaller, (g)Mold 4-bigger, (h)Mold 4-smaller

Figure 23 shows the averaged Stress-Strain curves for the seven different molds with auxetic structure plus the normal mold without any structure. As expected, the normal mold has by far the highest compressive strength and the highest young's modulus. The strongest structure beside of that is Mold 1 – 3 Rows, followed by Mold 1 – 4 Rows and Mold 4 -smaller. As to be seen in Table 1 these molds are the structures with the lowest void content. Just Mold 4 – bigger is missing in this ranking which probably comes from the fact that the arrows of Mold 4 have much more sharp edges than Mold 1 does. Furthermore, the tips of the arrows point to each other which can cause a crack much faster than the sides of the triangles that are turned towards each other. This probably also explains why Mold 4 - smaller is so much stronger than Mold 4 – bigger. As the arrows are closer together for the last-mentioned mold a crack occurs faster than for a bigger gap between the voids. Mold 2 is the weakest structure according to this chart.

This could be due to the corners of the diamonds that are relatively close together and facilitate stress concentrations and therefore a faster failure.

Regarding the comparison of the different variations of Mold 1, 3 and 4, it is observed that a lower void content leads to a higher compressive strength. An exception to this is Mold 3 that shows almost no difference between the two variations.

To summarize, of the compressive strength Mold 1 – 3 Rows is the most suitable structure for use in the construction industry, since its strength comes closest to a mold without voids.

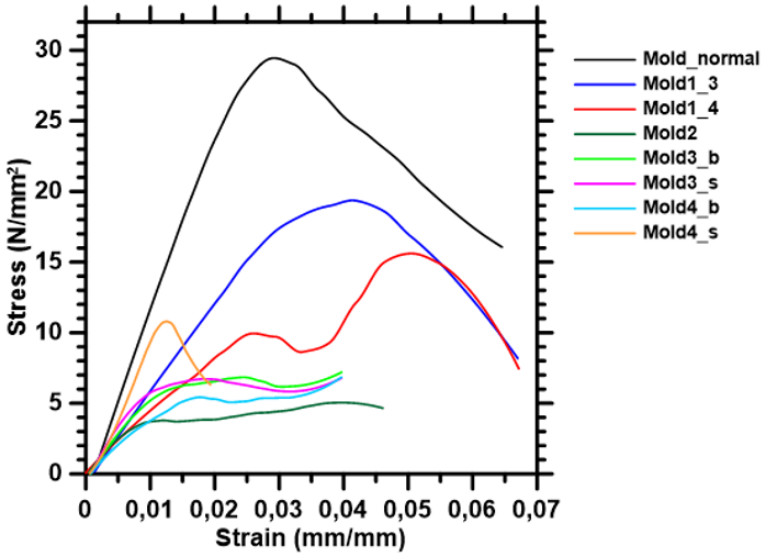

Figure 23: Averaged Stress-Strain Curves for all Molds

Auxetic Behavior

Auxetic behavior occurs if a negative Poisson's ratio is existent. This means for a compression test that the cube has to contract in longitudinal direction as it is compressed in axial direction. Since the displacement in the DIC software Ncorr is defined positive to the right in X direction and down in Y direction, negative displacement on

the right half of the cube and positive displacement on the left half of the cube has to occur to identify auxetic behavior. The expected DIC result is to be seen in Figure 24(b). For a cube that does not behave auxetic the exact opposite is expected. Figure 24 shows the U-displacement and V-displacement for Mold 2_3. The pictures show the expected result for a cube with auxetic behavior just the displacements are switched. That means that the U-displacement (Figure 24(a)) shows the expected displacement in Y-direction and the V-displacement (Figure 24(b)) shows the expected displacement in X direction.

A possible reason for this is again the concave and convex sides of the cube as it makes the cube move during compression. This could lead to a rotation during the experiment and these switched displacements as a result. Even though this could be a logical explanation it is very perplexing that the displacement is switched for every single mold without any exception and that all molds show a perfectly horizontal and vertical displacement just in the wrong displacement plot. Different time segments of the same experiment were analyzed with the DIC software to find the moment where the test specimen is not moving anymore and fixed between the two compression plates. It was obtained that the DIC is very dependent on the reference picture or on the point in time, where the analysis starts, respectively, especially for a difficult case like these experiments, but nothing worked out and showed a reasonable displacement. Another consideration was that the DIC software switches the axes for some reason during the experiment. A 3D printed plastic cube with 100% infill was tested to see if the same happens in this case but for this cube the displacements were the right way around.

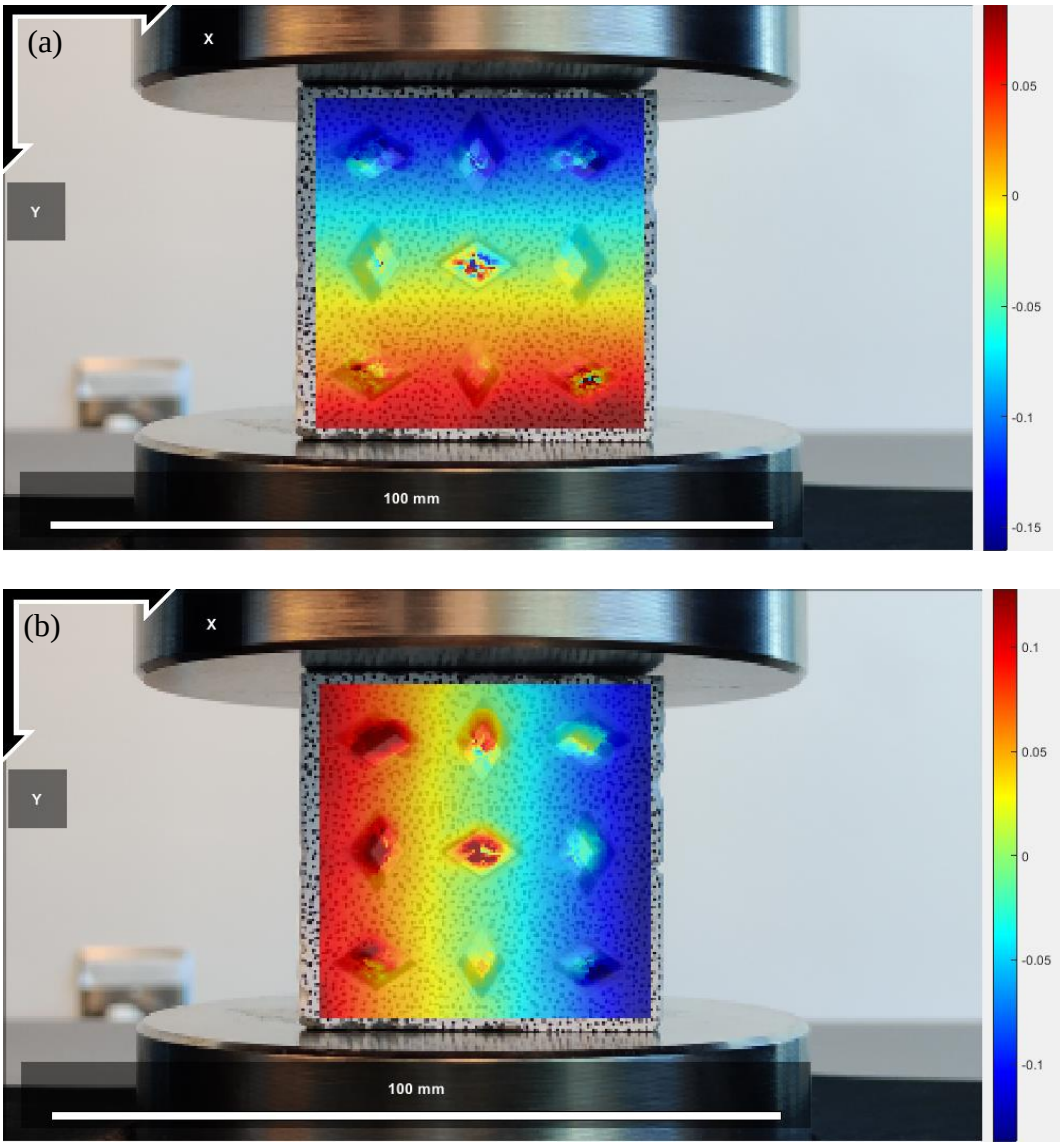

Figure 24: Displacement Compression Test in (a) X direction and (b) Y direction

As a verification three normal samples and one cube with the structure of Mold 2 were cast again to see if straight walls can change the result of the DIC software. For time reasons only these four samples could be created. For the normal molds a massive plastic mold was used and for Mold 2 a mold with two layers was printed to guarantee that no bulging can occur. Mold 2 was very difficult to demold but after 28 days the

molds could be painted and tested. Finally, Mold 2 showed the expected displacement in the right displacement plot in the DIC software as to be seen in Figure 25. Unfortunately, it does not show auxetic behavior as the cube expands in horizontal direction. This result shows that the problem is not in the software itself. On the other hand, all three full cubes of the normal mold showed very unclear behavior. For none of them the horizontal displacement could be obtained as the U-displacement was rotating and moving until it looked almost like the V displacement. To the best of the authors knowledge the elastic and linear section of the curve was chosen to prevent movement, the DIC parameters were set as they are supposed to be, and the dots were painted in a way so that the software never lost correlation.

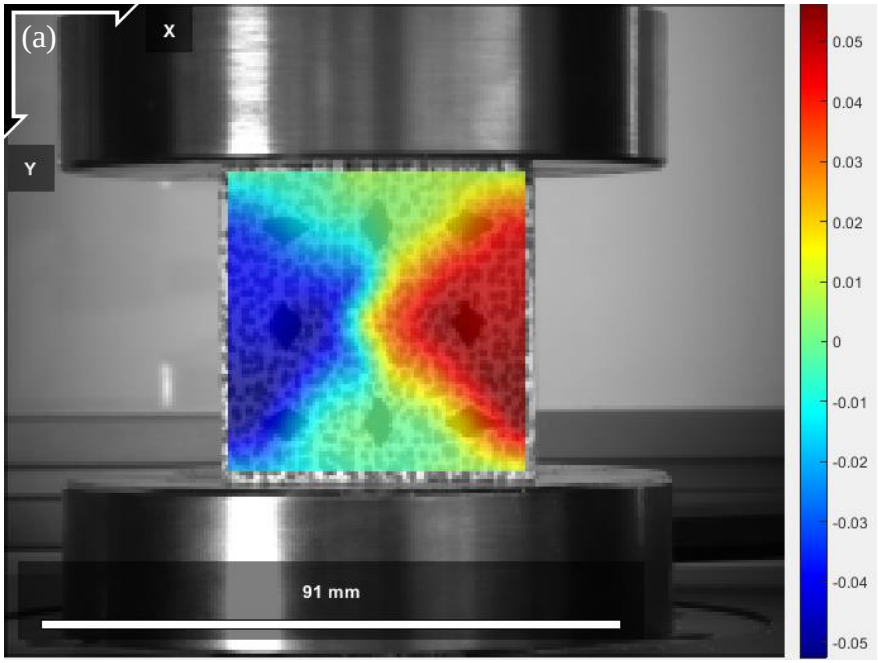

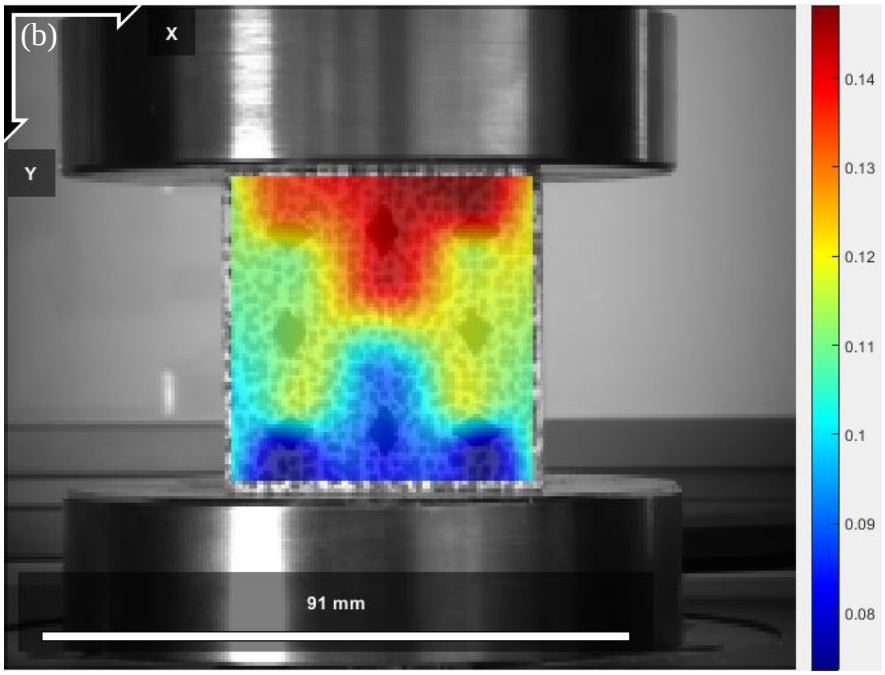

Figure 25: Displacements for Verification Cube in (a)X-direction and (b)Y-direction

Since it is still unclear why the displacements were the other way around and about half of the molds showed auxetic behavior in the V-displacement, which roughly corresponded to the expectations of these experiments, the results are presented here anyway. It should be noted that the assumption of whether auxetic behavior was achieved or not was made on the basis of the V-displacement, although it would actually have to be attached to the U-displacement. In order to rule out the possibility that the cubes expand or contract as a result of the convex or concave shape of their sides, the cubes were analyzed for their bulge and compared with their behavior in the X-direction. No correlation could be established. The results are presented in Table 4. The seven rows present the different structure types whereas the four columns list the specimens for each type. The bold written molds behaved auxetic according to the standards mentioned. It is obtained that for most of the structure types at least half of the samples behaved auxetic.

Mold 1-4 Rows and Mold 4-smaller appear to be the most auxetic ones. Only Mold 3 seems to behave rather not auxetic.

Table 4: Auxetic Behavior Cubes

Mold 1_3_1	**Mold 1_3_2**	**Mold 1_3_3**	Mold 1_3_4
Mold 1_4_1	Mold 1_4_2	**Mold 1_4_3**	**Mold 1_4_4**
Mold 2_1	Mold 2_2	**Mold 2_3**	
Mold 3_b_1	Mold 3_b_2	Mold 3_b_3	Mold 3_b_4
Mold 3_s_1	Mold 3_s_2	Mold 3_s_3	Mold 3_s_4
Mold 4_b_1	Mold 4_b_2	Mold 4_b_3	**Mold 4_b_4**
Mold 4_s_1	**Mold 4_s_2**	**Mold 4_s_3**	Mold 4_s_4

Three-Point-Bending Tests

As the results of the cubes regarding the auxetic behavior were not satisfying, 1% of fibers were added to the mortar mix of the beams to increase the deformation capability and the time between the beginning of loading and failure. For this reason, the loading rate was also reduced from 1mm/min to 0.375mm/min. Furthermore, the molds for the beams were printed with two layers instead of one to prevent bulges at the sides and increase the position stability during testing. For time reasons only three instead of four samples for each structure type could be created. The testing procedure is explained in the three-point-bending section.

Flexural Strength

As to be seen in Figure 26 the Force-Displacement results of the three-point bending tests are much closer together as the results from the compression tests. Most of the test specimen show a steep increase until failure, then the curve drops as a result of the crack and then it maintains the same level or decreases slowly. A good example for this is Mold_normal in Figure 26(a). All three samples peak around 2000 to 2300N, drop around 400 to 500 N and flatten out at around 1100N. On the other hand, the vertical displacement varies from 0.15mm to 0.4mm. On the contrary, Mold 1-3 Rows in Figure 26(b) shows a deflection of around 0.4mm for all three test specimen but the force at failure varies from 1600 to 2300N. The Force-Displacement curve of Mold 1-4 Rows in Figure 26(c) looks almost like a stress-strain curve for steel with a yield force between 1100 and 1400N and a maximum bearable force of 1200 or 1600N, respectively. While two of the Mold 2 samples in Figure 26(d) showed a similar behavior of a force of 1100N and a displacement of 0.4mm at failure, the third Mold shows a slow irregular increase until it fails at impressing 1.2mm of displacement and a force of 1550N. The curves of Mold 3-bigger in Figure 26(e) are very parallel to each other and fail between 1350 and 1600N and between 0.35 and 0.55mm of deflection, respectively. Mold 3-smaller in Figure 26(f) shows a big variation of results. The force varies from 1250 to 2000N and the displacement from 0.4 to 1.3mm. While the curves of Mold 4-smaller in Figure 26 are identical until the samples fail at different force levels between 1150 and 1600N at around 0.6mm of vertical displacement, Mold 4-bigger in Figure 26(g) all show a similar shape of the curve but at different force and displacement levels. The force varies from 1350 to 1900N and the displacement from 0.4 to 0.7mm.

The differences between the different samples of each structure type probably arise again from the not perfectly straight sides of the beam. Even though only some of the molds arched because of cooling problems during printing, the specimens were not exactly rectangular. The uniformity was better than for the cubes and furthermore, the beams had only a very small area of support in the three-point bending test, but it could still make a small difference. Another difficulty was the fiber distribution in the mortar mix because of all the small structures in the molds as already explained in the Casting and Demolding Section. Although the fibers were distributed as even as possible, the distribution could still have a big influence on the fracture behavior during the three-point-bending experiments.

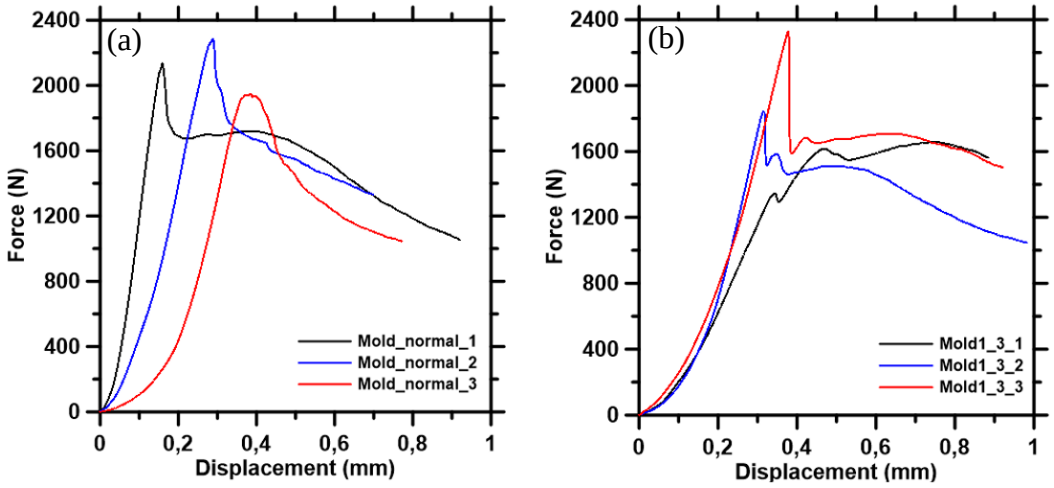

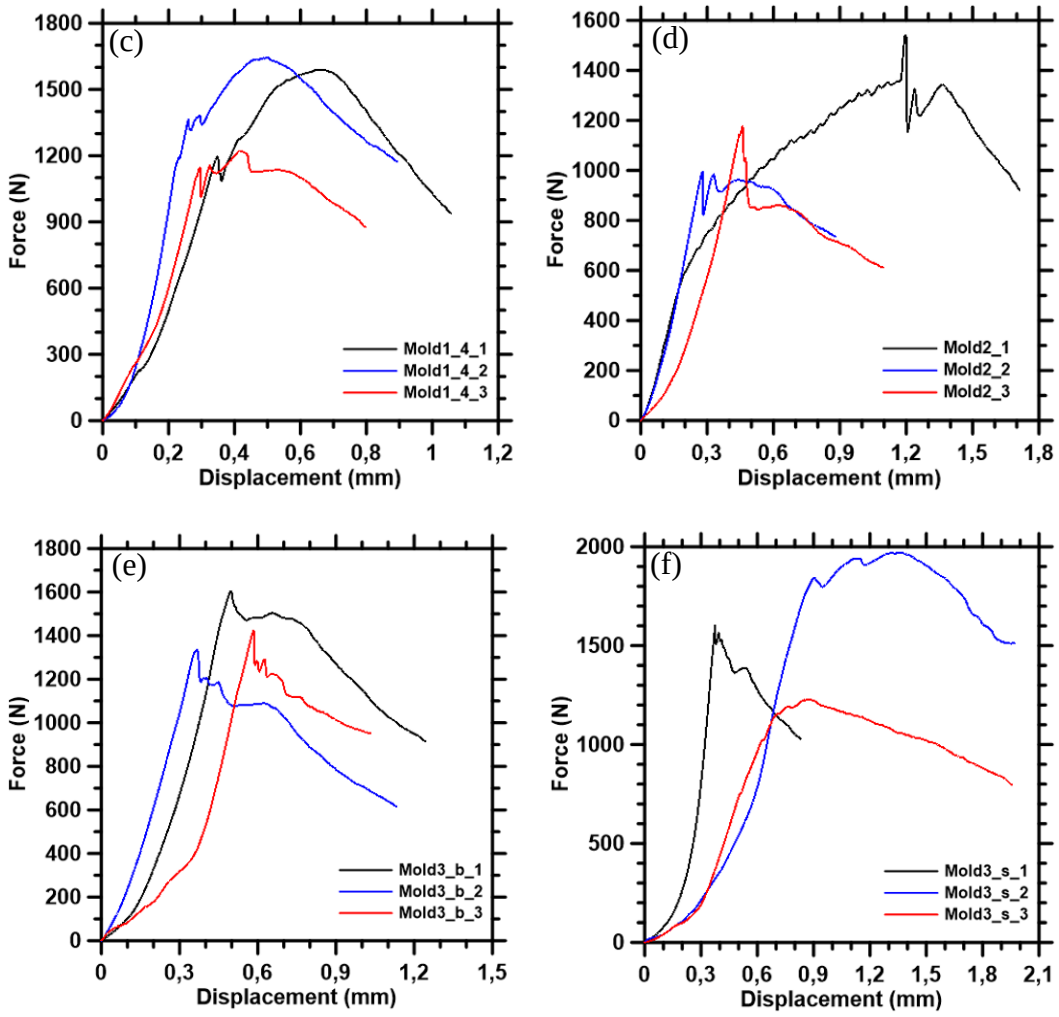
(c)
Force (N)
Displacement (mm)
Mold1_4_1
Mold1_4_2
Mold1_4_3
(d)
Force (N)
Displacement (mm)
Mold2_1
Mold2_2
Mold2_3
(e)
Force (N)
Displacement (mm)
Mold3_b_1
Mold3_b_2
Mold3_b_3
(f)
Force (N)
Displacement (mm)
Mold3_s_1
Mold3_s_2
Mold3_s_3

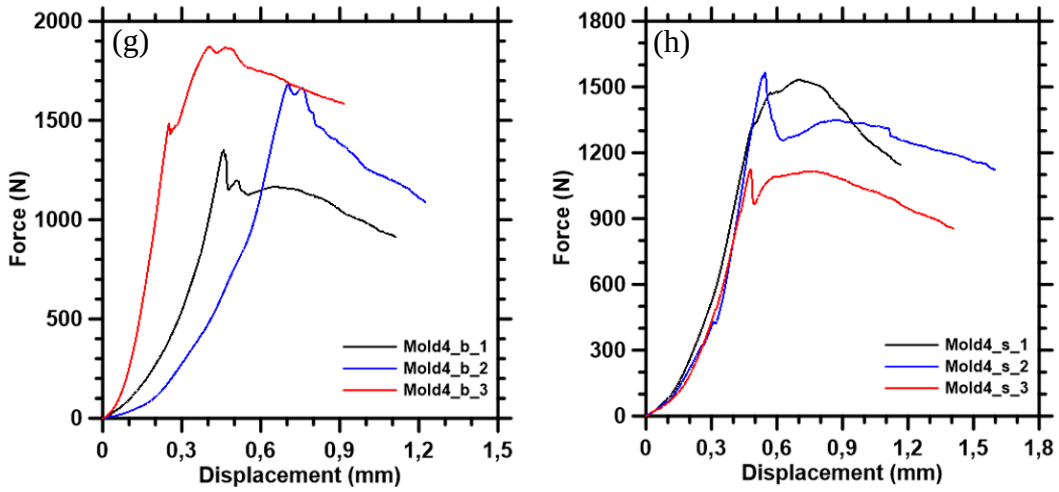

Figure 26: Force Displacement Curves for Three-Point-Bending Tests for (a)Mold normal, (b)Mold 1-3Rows, (c)Mold 1-4Rows, (d)Mold 2, (e)Mold 3-bigger, (f)Mold 3-smaller, (g)Mold 4-bigger, (h)Mold 4-smaller

Figure 27 is supposed to illustrate the differences between the various structure types. The left chart shows the force in Newton and the displacement in mm whereas the right chart represents the flexural strength in MPa and the displacement in mm. In comparison to the cubes these results are much closer together. The normal mold is still the strongest with around 4.3MPa but also had the smallest displacement of 0.35mm. The two strongest molds of the molds with voids are Mold 1-3 Rows and Mold 3-smaller with 3.9 and 3.7MPa, respectively. The weakest molds are Mold 3-bigger and Mold 4-smaller with 3.1 and 3.2MPa, respectively. This is kind of surprising as Mold 3-bigger is the mold with the highest void content but Mold 4-smaller is the one with the lowest void content and the distance between the lower edge of the beam and the first void where the crack occurs is also the biggest of all molds. The molds with voids with the lowest displacement at failure are Mold 1-3Rows and Mold 1-4Rows with 0.4 and 0.5mm, respectively, and the molds with the highest deflection are Mold 2 and Mold 3-smaller with 1.3mm and 1.1mm, respectively.

Regarding the comparison of the two variations of Mold 1, 3 and 4 most of them performed as expected concerning the flexural strength. As already mentioned, Mold 4-small was surprisingly weak and performed worse than the bigger variation of Mold 4 although in relation to the void content something else would have been expected. For Mold 1 and 3 the mold with the higher void content for each of the structures showed a lower flexural strength as expected. Nevertheless, it should be pointed out that although Mold 3-bigger had a lower maximum flexural strength as Mold 3-smaller, the displacement was also lower. Depending on the area of application in the construction industry, this can have a similar meaning as load-bearing capacity and should therefore not be overlooked.

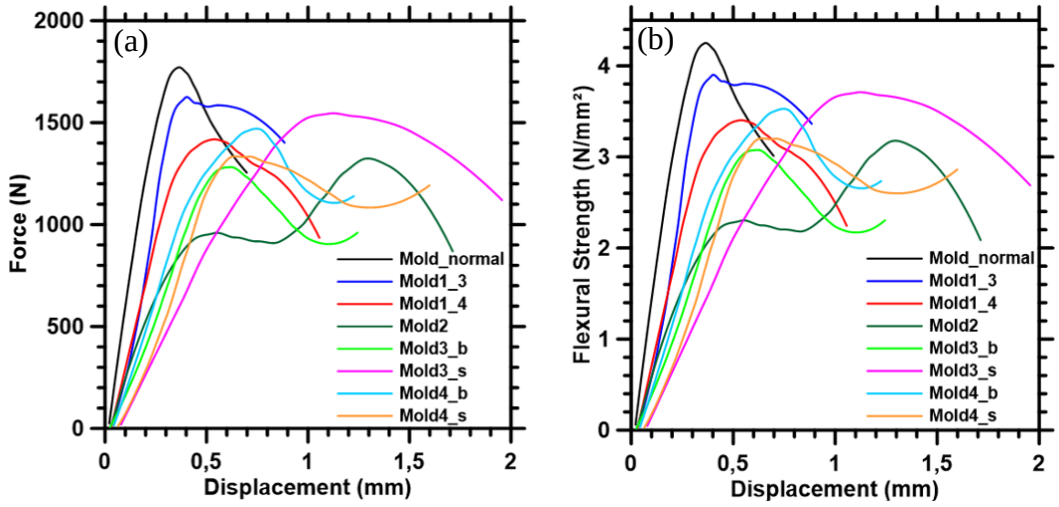

Figure 27: (a) Averaged Force-Displacement Curves for all Molds, (b) Averaged Flexural Strength-Displacement Curves for all Molds

In summary, regarding the flexural strength and the displacement at failure Mold 1-3Rows performed the best of all molds with voids and is almost comparable to the beam without any voids.

Auxetic Behavior

When a conventional beam made of mortar or concrete is tested in a three-point-bending machine, it bends particularly in the middle, while it barely moves on the end bearings apart from a slight rotation in response to the bending in the middle and thereby reduces the overhang a little. Due to the deflection, a conventional beam becomes narrower towards the middle. In contrast to this, a beam with auxetic behavior would become wider, thus expanding vertically towards the middle.

In order to find out whether auxetic behavior has been achieved, it is first necessary to determine how the displacement in the DIC software is supposed to look in case of auxetic behavior. For this purpose, it was considered that for a theoretical beam that does not expand or shrink, the deflection over the height of the beam remains constant and decreases from the center to the edge. With a Y-axis that is positively defined downwards, as is the case of the DIC software, and a conventional beam, the narrowing in the middle of the beam would mean that the displacement would have to be larger at the top of the beam and smaller at the bottom of the beam than at the center axis and would still decrease towards the edge. This results in a semicircle as shown in Figure 28(a). The exact opposite would happen for a beam with auxetic behavior. The expansion in the middle of the beam would cause a smaller displacement at the top of the beam and a larger displacement at the bottom of the beam than at the center axis and would decrease again towards the edge as to be seen in Figure 28(b).

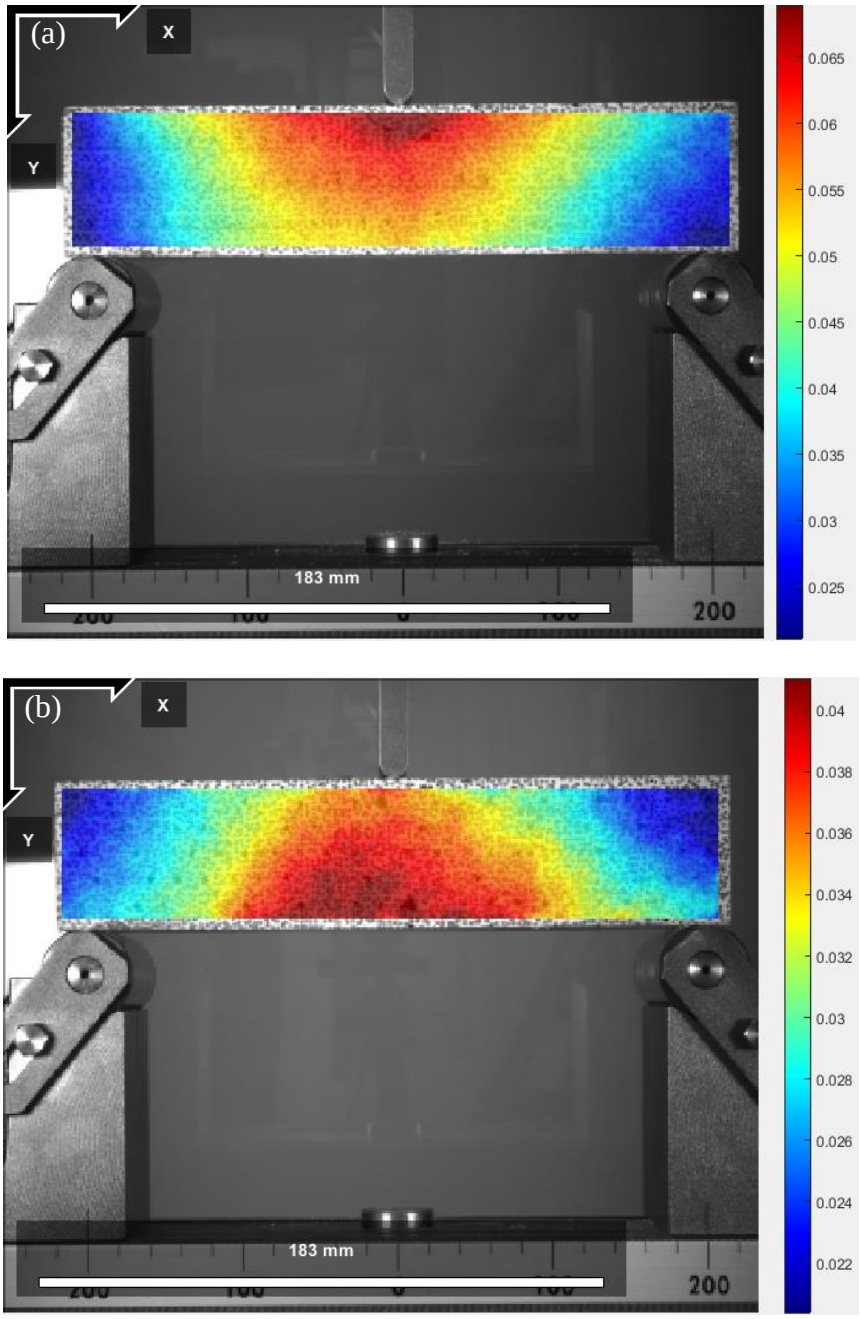

Figure 28: V-Displacements for Beams (a)without auxetic behavior and (b) with auxetic behavior

Even though the results were much more reasonable than the ones of the cubes, they were still not completely clear. It was expected that the pattern of the displacement stays almost the same during an experiment and the displacement slowly increases with

time and force, but this was not the case. For most of the samples the force was increasing very constantly as to be seen in Figure 26 and a few tenth of a millimeter of deflection could be identified. For the DIC only the linear part of the curve where no movement of the beam should occur anymore was chosen. But as the displacements were very small and the beams not perfectly rectangular the displacement changed considerably with every picture in the DIC, and it is not possible to say unequivocally how the beams have deformed. Another problem was that some of the beams were a little bit inclined on the pictures for the DIC because of the slightly uneven sides of the beam. A beam that is not exactly parallel to the X-axis makes it more difficult to read the results in the DIC because the displacements are only in X and Y direction.

In the light of such vague results, it was decided not to calculate the Poisson's ratio of the beams. Although it has to be mentioned that these results should be treated with caution, there are some beams that, at least according to the DIC analysis, show tendencies towards auxetic behavior. Therefore, these results are presented here (Table 5). The seven rows show the different structure types, and the three columns list the different specimens of each type. The bold written molds are test specimens that have shown auxetic behavior in the displacement results.

Table 5: Auxetic Behavior Beams

Mold 1_3_1	Mold 1_3_2	**Mold 1_3_3**
Mold 1_4_1	Mold 1_4_2	**Mold 1_4_3**
Mold 2_1	Mold 2_2	**Mold 2_3**
Mold 3_b_1	**Mold 3_b_2**	**Mold 3_b_3**
Mold 3_s_1	**Mold 3_s_2**	**Mold 3_s_3**
Mold 4_b_1	Mold 4_b_2	Mold 4_b_3
Mold 4_s_1	Mold 4_s_2	Mold 4_s_3

As to be seen in Table 5 Mold 3-bigger seems to be the most auxetic structure. This is surprising as this mold showed the least auxetic behavior in the compression tests. The next structures showing tendencies of auxetic behavior are Mold 1-3 Rows and Mold 3-smaller.

.

CHAPTER 5

VERIFICATION WITH SIMULATIONS

The experiments have not been able to make a clear statement whether or not auxetic behavior has occurred. In order to find out why the experiments did not work as expected, and to determine the parameters required for the auxetic behavior that the different molds were originally intended for, simulations were performed. The hypothesis was that a structure with repeating unit cells is needed to achieve auxetic behavior and that the thick edge around the voids of the created molds prevented the fracture behavior that is needed for an auxetic behavior. Therefore, similar to [18] a geometry with alternating horizontal and vertical ellipsoid voids was created. To identify requirements that are needed for achieving auxetic behavior, different parameters were chosen and varied for the simulations. The parameters were the aspect ratio, the length of the major axis and the number of voids along X and Y direction. The objective of the simulations was to find a structure that behaves auxetic to compare this with the structures that were used for the experiments to clarify why they did not work as expected. Furthermore, conditions that must be met in order to achieve auxetic behavior are to be identified so that one can repeat the experiments of this thesis and can actually verify auxetic mortar structures.

In addition, the simulations are used to create a prediction tool for the Poisson's ratio or auxetic behavior, respectively. The papers, explained in the Literature Review of this thesis, show that auxetic behavior of CCC is generally possible and highlight the

basic requirements to achieve this behavior. Some geometries that have a negative Poisson's ratio were found. What is still missing is an easy prediction tool for everyone. Auxetic properties such as shear and indention resistance and damping and fracture toughness are helpful characteristics in the building industry because they can improve the life-time and strength of the concrete component [13]. Materials with these innovative properties should not only stay subject of laboratory research but also be accessible to everyone in industry and the scientific community. As of now a FEA (finite element analysis) with simulations would be necessary to determine the Poisson's ratio and the degree of auxetic behavior. But not everyone is able to use these complex simulation tools. Besides, a simple and yet robust as well as user-friendly design tool would provide enormous value to the designers and decision-makers as they would be able to easily leverage such tools for performance tuning and risk assessment which is challenging to do with computationally exhaustive and complex FEA-based simulation tools. The goal of this work is to develop a machine learning based prediction tool for ACCC that is easy to use so that everyone can access the advantages of auxetics.

However, the development of a robust ML-based prediction tool requires a large, consistent and representative dataset which is currently not available for auxetic CCCs. Moreover, owing to the black-box nature of ML techniques such as neural network, its indiscriminate use can lead to non-physical solutions. Therefore, to address the aforementioned challenges, this study implements high-throughput FE simulations to obtain a large dataset of Poisson's ratio for varying mesoscale architectural features. The large dataset is leveraged for ML-based performance prediction. Integration of ML with FEA-based numerical simulation helps to maintain the fundamental laws of physics and to

avoid nonphysical solutions. This provides the opportunity that everyone can for example change the material properties at his convenience and gets an immediate response. Overall, the synergistically integrated high throughput FEA-based simulations and ML-based approach, that is based on the simulations explained in this chapter, is expected to enable materials engineers and decision makers to make intelligent, informed decisions regarding the selection of mesoscale architectural features in cellular cementitious composites to meet the desired performance goals. Thus, the design tools presented in this paper can accelerate the acceptance and utilization of auxetic cementitious cellular composites for a wide range of structural applications. This innovative platform will shift the use of ACCC from the laboratories and research into the world of the industry and practical applications and will open new doors for everyone.

In the following it is explained how the effective Poisson's ratio of the cellular cementitious composites is computed using finite element analysis. The forthcoming sub-sections first detail the numerical simulation methodology followed by response evaluations and large dataset generation.

Simulation Methodology

In this section, the numerical simulation framework towards the prediction of Poisson's ratio of the cellular cementitious composites with variating shape and dimension of voids is elaborated. The framework is schematically illustrated in Figure 29. The first step involves generating the periodic geometry for representative unit cells with elliptical voids. It is assumed that the geometry to be studied must be periodic in order to exhibit auxetic behavior. This means that the unit cell under study must be constructed in such a way that it can be connected to an infinite number of identical unit cells in all

directions, forming a larger geometry that is still auxetic. The variations of the Poisson's ratio are simulated by changing the aspect ratio of the elliptical voids, which is the ratio of the major axis to the minor axis, the length of the major axis, and the number of voids in the X and Y direction in the representative meso-structure. For each combination, the shape of each void in the meso-structure is maintained identical but the voids are alternate vertical and horizontal oriented. Similar observation is considered in the previous literature [15, 18]. Then the unit cells are meshed. An RVE Mesh Convergence Study is located in the Appendix. Afterwards, a Dirichlet boundary condition is chosen to mimic the free edges uniaxial compression test. A uniaxial strain at a finite rate is applied, and a longitudinal strain and a transverse strain response are obtained. Using a homogenization procedure and the linear relationship between the longitudinal strain and the transverse strain, Poisson's ratio is then computed. The analysis is carried out in ABAQUS^{TM} using python scripts for geometry generation and followed by a post-processing module coded in MATLAB. The following sub-sections further elaborate on the process for a comprehensive understanding.

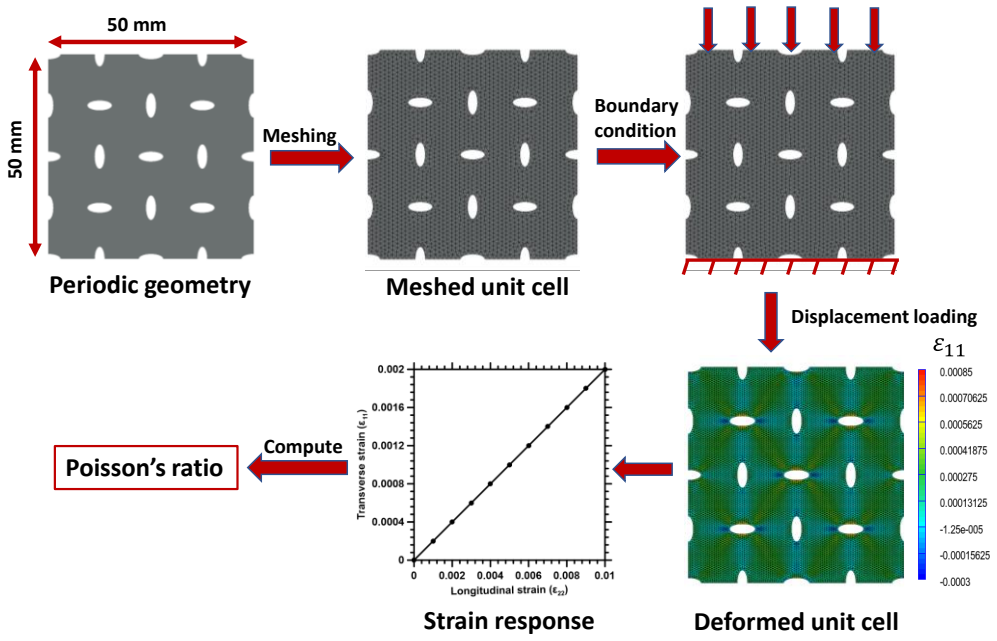

Figure 29: Schematic Representation of the Simulation Framework

Geometry Generation Approach, Model Geometry and Parametric Variations

The unit cell is generated by forming a grid with the desired number of voids along the X-axis and the Y-axis. The center points of the voids are placed by distributing the points with an equal space based on the size of the unit cell, which is 50mm in this study. Once, the points have been generated, unit circles around the points are added with a given diameter. For an aspect ratio greater than 1, the ellipse shape is developed by varying the unit circle with scale factors that correspond to the major and minor axes length or the major axis length and the aspect ratio. Since the elliptical shapes in this study are arranged alternately, as shown in Figure 30, two different voids with two different angles are applied at 0 degree and 90 degrees. These angles are necessary to rotate the ellipse accordingly. Since, the aspect ratio considered in this study is greater than or equal to 1, the maximum diameter or the maximum major axis length, respectively, is

varied until the distance between the center-to-center points is greater than the sum of one half of the major axis length and one half of the minor axis length of the ellipse and the minimum spacing allowed, which is 2mm in this study. The minimum diameter is decided by the user and is chosen to 6mm.

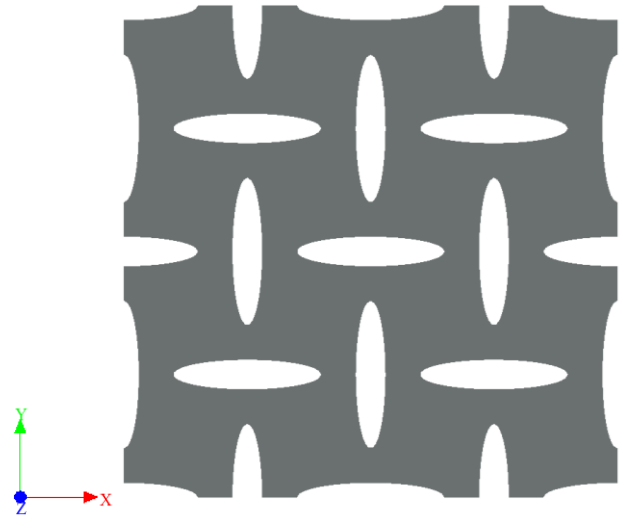

Figure 30: Representative Geometry of the Unit Cell Meso-structure

Table 6 describes the range of the parametric variations considered in this study. The ranges have been selected judiciously with a maximum void content of 50%. The aspect ratio, which is the ratio of the major axis to the minor axis is taken between 1 and 5. The aspect ratio adopted in the literature ranges from 1 to 3 [15, 18]. The minimum length of the major axis is 6mm whereas the maximum length of the major axis is 38.3mm. Considering the median diameter of 0.6mm for sand in mortar, the minimum void length of 6mm was chosen as smaller voids are challenging to create using standard 3D printers. The maximum length was calculated based on the width of the model equal to 50mm, the number of voids, the aspect ratio, respectively, and the minimum gap of 2mm between the voids. The interval between the minimum and the maximum length

of the major axis was subdivided uniformly into 10-20 values depending on the size of the interval. The smallest difference between two values that was assumed is 3mm, since smaller differences no longer have any influence on the result, and thus on the Poisson's ratio. The maximum number of voids along X-axis and Y-axis considered in this study is 8. The same value has also been adopted in the previous literature [15, 18]. This value was calculated by considering the spacing of 2mm, the aspect ratio, respectively, the width of the specimen equal to 50mm and the length of the major axis equal to 6mm as this will facilitate the highest possible number of voids.

Table 6: Mortar Model with Different Design Parameter Variations

Parameters	**Min**	**Max**
Aspect ratio	1	5
Length of major axis	6 mm	38.3 mm
Number of voids along X-direction (N_x)	2	8
Number of voids along Y-direction (N_y)	2	8

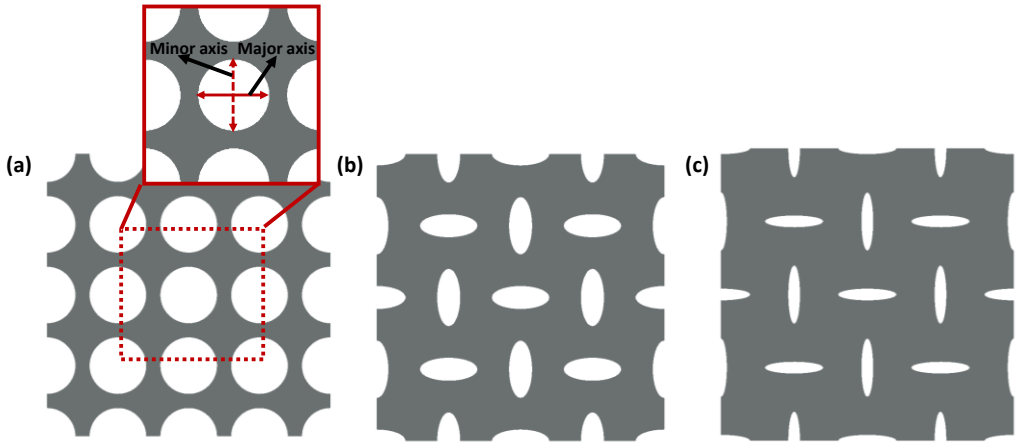

Figure 31: Model geometry with 6mm length of the major axis for an aspect ratio of (a) 1, (b) 2.5, (c) 4. The number of voids in x-direction and y-direction is identical and equals to 4

Figure 31 demonstrates the model geometry with various aspect ratios for a constant length of major axis, and the same number of voids along X-axis and Y-axis. The subfigure in Figure 31(a) indicates the minor axis and the major axis for one void. The major axis is always the longer axis. The minor axis is calculated by the length of the major axis divided by the aspect ratio. It can be seen that with constant number of voids and length of the major axis, the porosity decreases with increasing aspect ratio. Figure 32 depicts the model geometry with variations in the number of voids along the X-axis and Y-axis for a constant aspect ratio and length of the major axis.

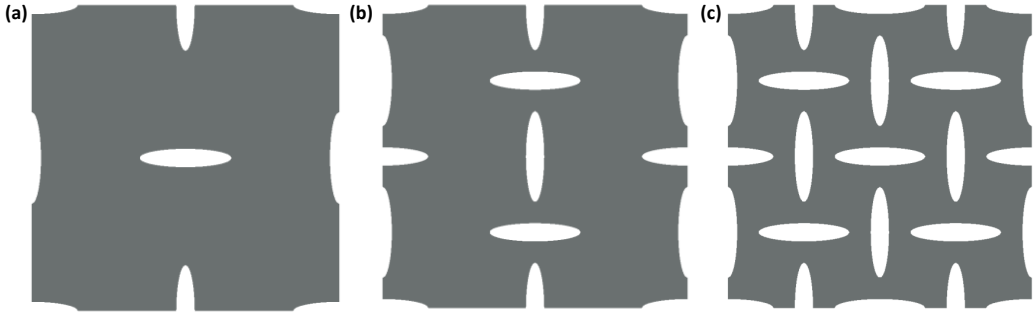

Figure 32: Model geometry with number of voids (a) N_x = 2 and N_y = 2, (b) N_x = 2 and N_y = 4, (c) N_x =4 and N_y = 4 for a constant aspect ratio of 5 and length of major axis = 15 mm. The number of voids in X-direction and Y-direction is denoted as N_x and N_y, respectively

In this case, the porosity increases with the increase in the number of voids along the two axes. Figure 33 illustrates the change in the model geometry when the length of major axis increases for a constant aspect ratio and number of voids. The porosity increases with increasing length of the major axis. All these variations can certainly change the response behavior of the structure and impart auxetic nature from the structural response, which is the key objective of this study.

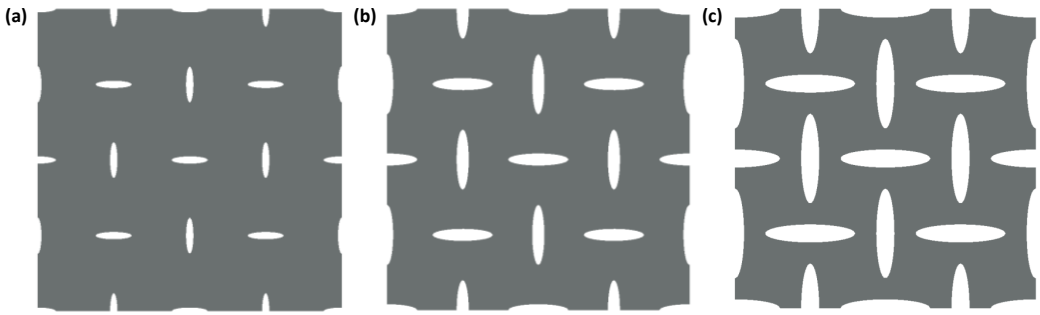

Figure 33: Model geometry for the major axis length of (a) 6 mm, (b) 10 mm and (c) 15 mm with a constant aspect ratio of 5 and number of voids in X-direction and Y-direction is identical and equals to 4

Material properties and boundary conditions

In this study, a linear elastic isotropic material is considered for the mortar with a Young's modulus of 25GPa and a Poisson's ratio of 0.18 [27]. This is necessary as one of the objectives is to explore the negative Poisson's ratio by introducing porosities in the geometry. This Poisson's ratio is not to be confused with the Poisson's ratio of the auxetic mortars with void content which is to be determined by the simulations. 0.18 is the Poisson's ratio of the mortar itself, while the Poisson's ratio to be determined represents the behavior of the auxetic structure of the test object. This Poisson's ratio is needed to identify auxetic behavior. Since the objective of this study is to evaluate the prospects of the negative Poisson's ratio by judiciously placing the elliptical voids in the geometry, the post-peak response and the effect of plasticity are not considered herein. A Dirichlet boundary condition is used, where the bottom edge is fixed, the loading is applied at the top edge, and the sides edges are unconstrained. Similar boundary condition is also considered in the previous literature [15, 18] to mimic the experimental uniaxial compression loading.

Effective response prediction

After the generated geometries are successfully meshed and the boundary conditions are applied, the geometries are subjected to uniaxial compression loading at the top edge with the loading speed lying in the quasi-static range (1e-4/s). At every loading step, the longitudinal strain (ε_L) and the transverse strain (ε_T) is computed. From there the effective Poisson's ratio (ϑ) is determined, which is expressed as

$$\vartheta = -\frac{\varepsilon_T}{\varepsilon_L}$$

In addition, the expression of the Poisson's ratio defined in this equation is valid as long as the transverse strain response is linearly correlated with the longitudinal strain.

Simulation Results and Dataset Generation for Machine Learning

This section shows the stress-strain results of the finite element analysis. From the illustrations it is possible to deduce whether auxetic behavior has occurred. After that the influence of the aspect ratio and the void contents are discussed as an interpretation of the finite element results. In a final step the displacements of the simulated auxetic structures are obtained and compared to the results of the performed experiments of this thesis. Finite element analysis is used later to generate a large and consistent dataset for ML implementation.

Simulated Stress-strain Responses

Figure 34 shows the stress distribution obtained at different strain states with increasing compressive loading. In voids where the main axis is horizontally aligned, tensile stresses are predominantly present, as indicated by the red color, whereas in voids where the main axis is vertically aligned, stress concentrations are observed along the

loading direction, as indicated by the blue color. Similar observations can be made for the strain concentration in Figure 35. For this particular pattern, a high compressive stress and strain is identified for voids closer to the loading and fixed edges, whereas a high tensile stress and strain are observed at the center as shown in Figure 34(c) and Figure 35(c).

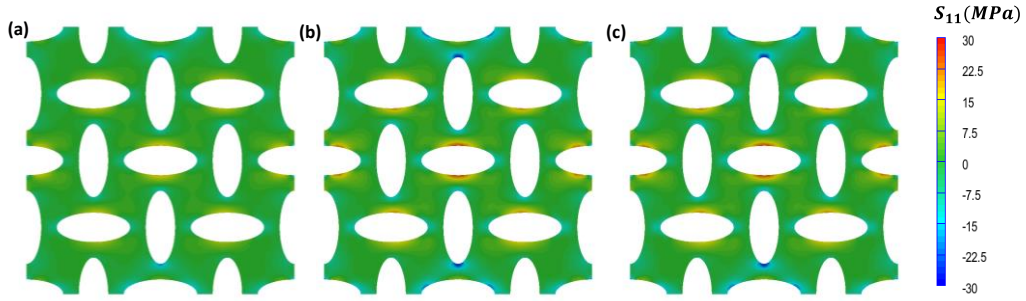

Figure 34: Stress distribution in the unit cell with (a) strain equals to 0.4 milli-strain, (b) strain equals to 0.7 milli-strain and (c) strain equals to 1 milli-strain

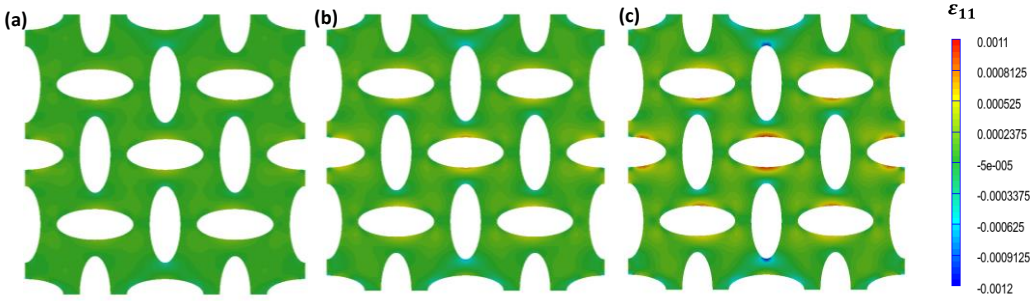

Figure 35: Strain distribution in the unit cell with (a) strain equals to 0.4 milli-strain, (b) strain equals to 0.7 milli-strain and (c) strain equals to 1 milli-strain

Influence of Aspect Ratio

To illustrate the influence of the aspect ratio on the auxetic response, Figure 36 plots the Poisson's ratio with varying aspect ratio and length of the major axis of the voids for various combinations of number of voids along X-axis and Y-axis. The number of voids is increasing from 2 voids in both directions in Figure 36(a) to 4 voids in both directions in Figure 36(c). It is observed that as the number of voids increases, the

distribution of the Poisson's ratio in general increases and especially the negative Poisson's ratio is widely distributed as shown in Figure 36(c). For a small number of voids (Figure 36(a)), the distribution is sensitive to increasing length of major axis irrespective of the aspect ratio. It can also be detected that irrespective of the aspect ratio, negative Poisson's ratio can be obtained with increasing length of major axis. However, it was also observed that the influence of the aspect ratio on the Poisson's ratio increases with increasing number of voids. Thus, with increasing length of the major axis and increasing void number, the difference of the Poisson's ratio between low and high aspect ratios increases significantly.

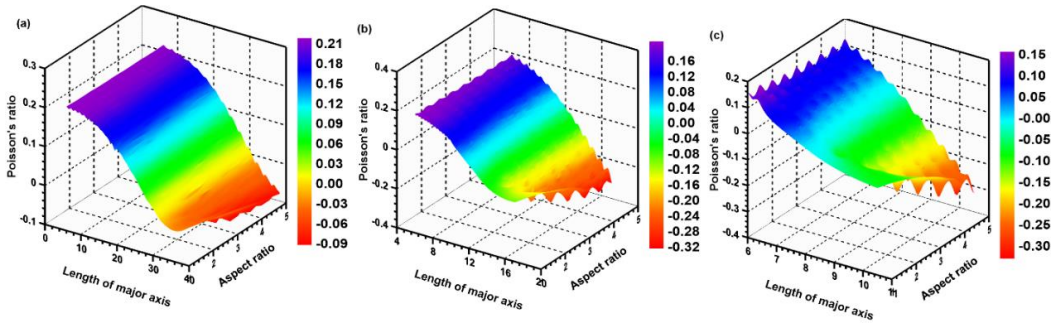

Figure 36: Response surface showing the influence of aspect ratio and length of major axis for (a) N_x = 2 and N_y = 2, (b) N_x = 2 and N_y = 4, (c) N_x =4 and N_y = 4 on Poisson's ratio

Influence of Void Contents

In this section, the influence of void contents on the Poisson's ratio in the form of number of voids along X-axis and Y-axis is demonstrated. Figure 37(a), (b) and (c) exhibit the 3D plots of Poisson's ratio distributions with varying number of voids along X and Y-axis for aspect ratios 3,4 and 5 respectively while keeping the length of the major axis fixed at 7.5mm. It is observed that the negative Poisson's ratio is narrowly

distributed towards higher number of voids (as shown in Figure 37). Hence, a high number of voids in both directions is required to achieve a negative Poisson's ratio and auxetic behavior, respectively. Although, the Poisson's ratio seems to be independent of the aspect ratio for a small number of voids, the Poisson's ratio for a high number of voids decreases significantly faster with increasing aspect ratio. For a higher aspect ratio, negative Poisson's ratio with the number of voids greater than 4 can be obtained (as shown in Figure 37(c)).

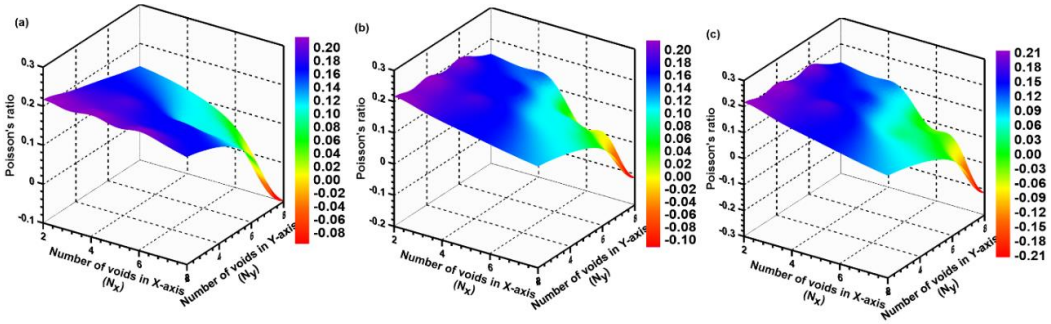

Figure 37: Response surface showing the influence of number of voids along X-axis (N_x) and number of voids along Y-axis (N_y) with length of major axis equals to 7.5mm for aspect ratio of (a) 3, (b) 4 and (c) 5 on Poisson's ratio

Displacement Results

Of all simulated geometries the one with a graticule of 6 times 6 voids, each with a length of 10.5mm and an aspect ratio of 5 was the most auxetic one. The void content could be determined to be around 25% and the Poisson's ratio was computed to -0.33. The simulated displacement for this geometry is shown in Figure 38. The simulated experiment was the same experiment as the compression tests that were performed for this thesis. The result thus shows the displacements that would have been expected in the compression tests just for another geometry. As to be seen in Figure 38(a) positive U-displacement can be obtained on the left half of the cube and negative displacement

on the right half. As the displacement is defined positive in the right direction, this results in a contraction of the cube in horizontal direction. Auxetic behavior has been achieved. Figure 38(b) illustrates the V-displacement. As specified in the boundary conditions, the bottom of the specimen is fixed similar to the experimental uniaxial compression test. Since the upward displacement is defined positive, the test specimen is being compressed.

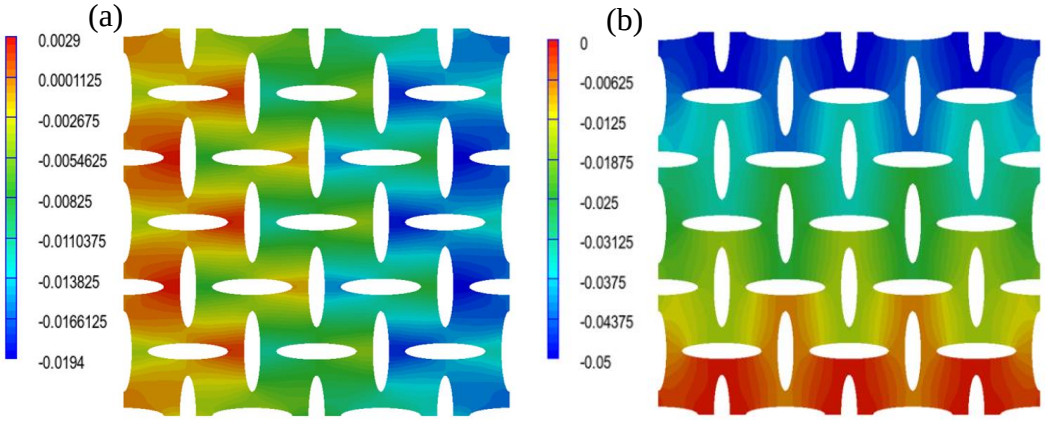

Figure 38: Simulated displacements in (a)X-direction and (b)Y-direction

From these results a few conclusions can be drawn about the performed experiments. First of all, the hypothesis of needing a repeating unit cell to achieve auxetic behavior seems to have turned out to be correct. Another detected problem regarding the evaluation of the results was that a lot of the simulated geometries showed a reduced Poisson's ratio in comparison to conventional mortar cubes, that was still not negative. In the experiments it was only searched for a negative Poisson's ratio as this is much easier to see even though a reduction of the Poisson's ratio could have been occurred for some of the molds. This could have shown at least the tendency of auxetic behavior. As already explained in the last sections, a high void content and/or aspect ratio is

needed to obtain a negative Poisson's ratio. The cubes were probably just too massive and the gaps between the voids too big to enable the required deformation for auxetic behavior. Together with the analysis of the influence of the aspect ratio and the void contents in the previous sections it should now be possible to create a mold for a mortar sample with the procedure described in this thesis that actually shows auxetic behavior.

.

CHAPTER 6

CONCLUSIONS AND FUTURE WORK

In this thesis a procedure was developed to create mortar samples with different auxetic structures. At first already existing auxetic structures were adapted to the special characteristics of mortar. The method of printing the molds was optimized and a suitable mortar mixture was evolved until the test specimen could be cast and demolded. They were tested in compression and three-point bending tests and the results were evaluated regarding the compressive and flexural strength, respectively, and the auxetic behavior using the DIC method. Differences between the different structures were worked out. As the experiments only showed vague results, a verification with simulations using finite element analysis was executed. The simulations were performed on an ellipsoid structure with varying parameters to find a structure that behaves auxetic and to identify the requirements for auxetic behavior. The parameters were the aspect ratio, the length of the major axis and the number of voids along X and Y direction. The influence of these parameters on the Poisson's ratio was determined and depicted. Furthermore, the most auxetic simulated geometry was identified, represented, and compared to the structures used for the experiments to understand why they remained below expectations.

From all this research several deductions can be drawn: First of all, a repeating unit cell is necessary to achieve auxetic behavior. A thick edge around the voids frustrated the required deformation and rotation for a negative Poisson's ratio. The fibers are supposed to ensure a deformation without failing the structure. PLA has proven to be the most manageable printing material for the molds, as it is easy to print, not too flexible

but still easy to demold. When printing the molds, attention has to be paid that the plastic shell does not deform due to cooling problems as this can change the test results. Therefore, at least two layers should be used for the shell. Especially for the cubes this significantly complicates the demolding process. Possibly other tools would have to be used for this. Furthermore, at least 1% of fibers should be added to the mortar mixture to obtain a crack bridging ability, as the rotation necessitates the structure to carry tensile as well as compressive loads.

Since the determination of the deformation of the specimen during testing using the DIC method is key for discovering auxetic behavior, a technique was evolved to paint the required dots on the samples. While painting the dots with a pen is very time-consuming, the novel technique of using a handheld printer for printing the black dots on the white covered test specimen takes only a few minutes and is still affordable.

Regarding the elaboration of the experiment results and the comparison of the different structures, Mold 1-3Rows (Figure 5) seems to be the strongest one in the compression test as well as in the three-point bending test. The vertical displacement at failure was around 0.4mm and the flexural strength of 3.9MPa was almost as high as for a conventional beam without voids, even though this mold has a void content of over 13%. The compressive strength of almost 20MPa was much smaller than for a cube without voids but it was still clearly stronger than the other structures. Also, for the auxetic behavior Mold 1-3Rows was one of the structures with the most tendencies to a negative Poisson's ratio even if these results are not completely reliable. In total, especially for bending components the re-entrant honeycomb structure modified for the particular properties of mortar seems to be a good alternative to the conventional material. Weight

and material can be saved, and thus costs can be reduced. Furthermore, the structure already showed tendencies to a negative Poisson's ratio so only a few modifications might be needed to achieve auxetic behavior.

The simulation results show that the Poisson's ratio is significantly decreasing with increasing number of voids and the length of the major axis. A high aspect ratio is not necessary to achieve auxetic behavior but can decrease the Poisson's ratio even more. The structure with the lowest Poisson's ratio of all simulated models was the geometry with 6 times 6 voids, each with a length of 10.5mm and an aspect ratio of 5. A Poisson's ratio of -0.33 was obtained.

This geometry can be used for future work to repeat the procedure that was developed in this thesis of creating samples and testing them to proof the simulations and achieve auxetic behavior in an actual experiment. The identified influence of the aspect ratio and the void content on the Poisson's ratio can be used as a requirement for auxetic behavior and applied on different geometries to develop more auxetic structures. As ACCC is an innovative material that provides completely new opportunities it should not exclusively remain subject of research but should be made accessible to everyone and applied in the practice of the building industry. To facilitate this intention and as already mentioned, the simulations will be used to develop a prediction tool based on machine learning, that enables everyone to predict the Poisson's ratio without any knowledge about finite element analysis or simulations. Furthermore, it would be reasonable to improve the procedure of creating samples with auxetic structures as it is very time-consuming and challenging especially for components in a big scale. One idea would be to use a 3D printer that can print the mortar itself so that printing a mold and

casting and demolding the mortar is not necessary anymore [28]. This would accelerate and facilitate the process significantly but needs more research in terms of the printer itself and the admixtures that allow high flowability during printing and a fast hardening after printing. Furthermore, an opportunity needs to be investigated to carry the tensile loads in large scale components as the fibers used for the experiments are not applicable for this anymore. A new approach found by the TU Delft [29] is to use auxetic concrete for breakwaters to relate the flexibility of the concrete to the movement of the waves for producing energy. This in particular is innovative, because it can change the opinion of the public about concrete from pollution due to CO_2 emissions to an eco-friendly renewable energy.

In summary, auxetic cementitious cellular composites are still in their infancy but already indicate innovative characteristics that can, if further investigated, lead to completely new areas of application for concrete.

APPENDIX

RVE Mesh Convergence Study

In order to show that the effective properties obtained using finite element analysis is converged, a mesh-convergence study for the representative unit cell of mortar meso-structure is carried out. Figure 39 shows the results of the mesh-convergence study. The goal is, to find a number of elements that satisfies a sufficient grade of accuracy and simultaneously optimizes the time feasibility. A mesh beyond 12491 4-node bilinear, reduced integration elements (CPE4R in ABAQUS), yields a converged solution. Thus, a total of 12491 elements are implemented. Thereby, the chosen element number of elements adequately capturing the effective Poisson's ratio of the unit cell. The chosen elements invoke a trade-off between computational expense and prediction efficiency.

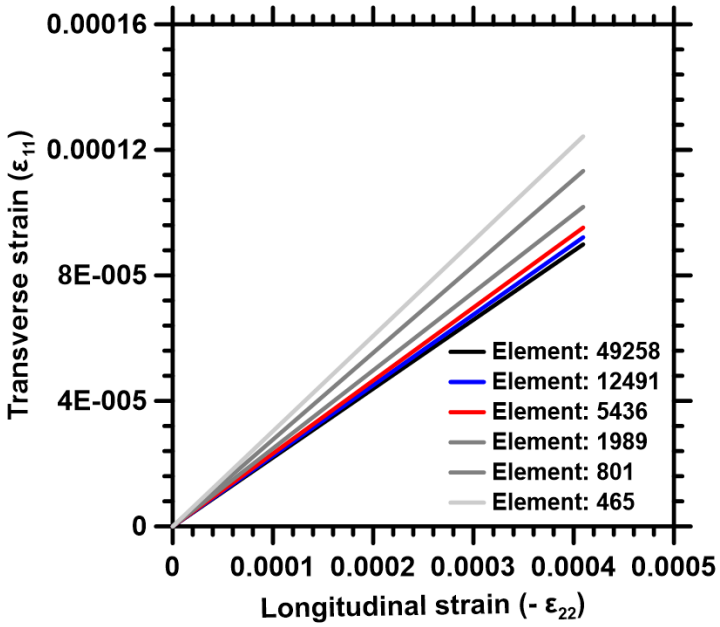

Figure 39: Mesh Convergence

REFERENCES

[1] F. Bos, R. Wolfs, Z. Ahmed, and T. Salet, "Additive manufacturing of concrete in construction: potentials and challenges of 3D concrete printing," *Virtual and Physical Prototyping*, vol. 11, no. 3, pp. 209–225, 2016.

[2] P. K. Mehta and P. J. M. Monteiro, *Concrete: Microstructure, properties, and materials*, 4th ed. New York, NY: McGraw-Hill Education, 2014.

[3] F. Lavergne, R. Belhadi, J. Carriat, and A. Ben Fraj, "Effect of nano-silica particles on the hydration, the rheology and the strength development of a blended cement paste," *Cement and Concrete Composites*, vol. 95, pp. 42–55, 2019.

[4] C. Herrera-Mesen, R. P. Salvador, S. Cavalaro, and A. Aguado, "Effect of gypsum content in sprayed cementitious matrices: Early age hydration and mechanical properties," *Cement and Concrete Composites*, vol. 95, pp. 81–91, 2019.

[5] D.-Y. Yoo and N. Banthia, "Mechanical properties of ultra-high-performance fiber-reinforced concrete: A review," *Cement and Concrete Composites*, vol. 73, pp. 267–280, 2016.

[6] H. Savastano, S. F. Santos, M. Radonjic, and W. O. Soboyejo, "Fracture and fatigue of natural fiber-reinforced cementitious composites," *Cement and Concrete Composites*, vol. 31, no. 4, pp. 232–243, 2009.

[7] J. Y. Yoon and J. H. Kim, “Mechanical properties of preplaced lightweight aggregates concrete,” *Construction and Building Materials*, vol. 216, pp. 440–449, 2019.

[8] I. Rahmouni, G. Promis, A. R'mili, H. Beji, and O. Limam, “Effect of carbonated aggregates on the mechanical properties and thermal conductivity of eco-concrete,” *Construction and Building Materials*, vol. 197, pp. 241–250, https://www.sciencedirect.com/science/article/pii/S0950061818329039, 2019.

[9] L. G. Li, C. J. Lin, G. M. Chen, A. Kwan, and T. Jiang, “Effects of packing on compressive behaviour of recycled aggregate concrete,” *Construction and Building Materials*, vol. 157, pp. 757–777, 2017.

[10] F. Özcan and M. Emin Koç, “Influence of ground pumice on compressive strength and air content of both non-air and air entrained concrete in fresh and hardened state,” *Construction and Building Materials*, vol. 187, pp. 382–393, 2018.

[11] M. Qiao, J. Chen, C. Yu, S. Wu, N. Gao, and Q. Ran, “Gemini surfactants as novel air entraining agents for concrete,” *Cement and Concrete Research*, vol. 100, pp. 40–46, 2017.

[12] K. E. Evans, “Auxetic polymers: a new range of materials,” *Endeavour*, vol. 15, no. 4, pp. 170–174, http://www.sciencedirect.com/science/article/pii/016093279190123S, 1991.

[13] Gabriel Stern, Aparna Deshmukh, Dr. Konstantin Sobolev, *3D Printing of Auxetic Concrete.* [Online] Available: http://poster.cae.uwm.edu/poster/sites/default/files/webform/submit_poster/393/p

oster2020-stern-gabriel-3d-printing-of-auxetic-concrete.pdf. Accessed on: Jan. 22 2021.

[14] X. Ren, R. Das, P. Tran, T. D. Ngo, and Y. M. Xie, “Auxetic metamaterials and structures: a review,” (en), *Smart Mater. Struct.*, vol. 27, no. 2, p. 23001, https://iopscience.iop.org/article/10.1088/1361-665X/aaa61c/meta, 2018.

[15] Y. Xu, H. Zhang, E. Schlangen, M. Luković, and B. Šavija, “Cementitious cellular composites with auxetic behavior,” *Cement and Concrete Composites*, vol. 111, p. 103624, 2020.

[16] H. Cho, D. Seo, and D.-N. Kim, “Mechanics of Auxetic Materials,” in *Handbook of Mechanics of Materials*, S. Schmauder, C.-S. Chen, and K. K. Chawla, Eds., Singapore: Springer Singapore, 2019, pp. 733–757.

[17] E. P. Hadjigeorgiou and G. E. Stavroulakis, “The Use of Auxetic Materials in Smart Structures,” *CMST*, vol. 10, no. 2, pp. 147–160, 2004.

[18] Y. Xu, E. Schlangen, M. Luković, and B. Šavija, “Tunable mechanical behavior of auxetic cementitious cellular composites (CCCs): Experiments and simulations,” *Construction and Building Materials*, vol. 266, p. 121388, 2021.

[19] H. Zhou, K. Jia, X. Wang, M.-X. Xiong, and Y. Wang, “Experimental and numerical investigation of low velocity impact response of foam concrete filled auxetic honeycombs,” *Thin-Walled Structures*, vol. 154, p. 106898, https://www.sciencedirect.com/science/article/pii/S026382312030776X, 2020.

[20] Yanping Liu and Hong Hu, “A review on auxetic structures and polymeric materials,” *Scientific Research and Essays*, vol. 5, no. 10, pp. 1052–1063,

https://www.researchgate.net/publication/273889759_A_review_on_auxetic_structures_and_polymeric_materials, 2010.

[21] *Test Method for Compressive Strength of Hydraulic Cement Mortars (Using 2-in. or [50-mm] Cube Specimens)*, ASTM C109/C109M - 20b.

[22] *Test Method for Flexural Strength of Concrete (Using Simple Beam with Third-Point Loading)*, ASTM C78/C78M - 21.

[23] N. McCormick and J. Lord, "Digital Image Correlation," *Materials Today*, vol. 13, no. 12, pp. 52–54, https://www.sciencedirect.com/science/article/pii/S1369702110702352, 2010.

[24] *https://digitalimagecorrelation.org.* [Online] Available: https://digitalimagecorrelation.org/. Accessed on: Jul. 28 2021.

[25] G. Mishra, "Why do We Test Concrete Compressive Strength after 28 Days?," *The Constructor*, 13 Aug., 2014, https://theconstructor.org/concrete/why-we-test-concrete-strength-after-28-days/6060/.

[26] Wikipedia, *Local regression.* [Online] Available: https://en.wikipedia.org/w/index.php?title=Local_regression&oldid=1029637107. Accessed on: Jul. 10 2021.

[27] F. Belabdelouahab, H. Trouzine, H. Hellal, B. Rahali, S. O. Kaci, and M. Medine, "Comparative Analysis of Estimated Young's Modulus of Rubberized Mortar and Concrete," (En;en), *Int J Civ Eng*, vol. 16, no. 2, pp. 243–253, https://link.springer.com/article/10.1007/s40999-016-0119-x, 2018.

[28] *3D printing of auxetic architecture element with cement paste ink - YouTube.* [Online] Available: https://www.youtube.com/watch?v=peMsMeA2CNI. Accessed on: Jan. 29 2021.

[29] TU Delft, *Obtaining energy from concrete.* [Online] Available: https://www.tudelft.nl/en/2021/citg/obtaining-energy-from-concrete. Accessed on: Jul. 12 2021.

BIBLIOGRAPHY

3D printing of auxetic architecture element with cement paste ink - YouTube. (n.d.). Retrieved 29.01.2021, from https://www.youtube.com/watch?v=peMsMeA2CNI

Amario, M., Rangel, C. S., Pepe, M., & Toledo Filho, R. D. (2017). Optimization of normal and high strength recycled aggregate concrete mixtures by using packing model. *Cement and Concrete Composites, 84*, pp. 83–92.

Belabdelouahab, F., Trouzine, H., Hellal, H., Rahali, B., Kaci, S. O., & Medine, M. (2018). Comparative Analysis of Estimated Young's Modulus of Rubberized Mortar and Concrete. *International Journal of Civil Engineering, 16*(2), pp. 243–253.

Bos, F., Wolfs, R., Ahmed, Z., & Salet, T. (2016). Additive manufacturing of concrete in construction: potentials and challenges of 3D concrete printing. *Virtual and Physical Prototyping, 11*(3), pp. 209–225.

Cho, H., Seo, D., & Kim, D.-N. (2019). Mechanics of Auxetic Materials. In S. Schmauder, C.-S. Chen, & K. K. Chawla, *Handbook of Mechanics of Materials* (pp. 733–757). Singapore: Springer Singapore.

Evans, K. E. (1991). Auxetic polymers: a new range of materials. *Endeavour*, *15*(4), pp. 170–174.

Gabriel Stern, Aparna Deshmukh, Dr. Konstantin Sobolev. (2020). *3D Printing of Auxetic Concrete*. (Department of Civil & Environmental Engineering, University of Wisconsin-Milwaukee, Producer) Retrieved 1 22, 2021, from http://poster.cae.uwm.edu/poster/sites/default/files/webform/submit_poster/393/poster2020-stern-gabriel-3d-printing-of-auxetic-concrete.pdf

Grima, J. N., Chetcuti, E., Manicaro, E., Attard, D., Camilleri, M., Gatt, R., & Evans, K. E. (2012). On the auxetic properties of generic rotating rigid triangles. *Proceedings of the Royal Society A: Mathematical, Physical and Engineering Sciences, 468*(2139), pp. 810–830.

Hadjigeorgiou, E. P., & Stavroulakis, G. E. (2004). The Use of Auxetic Materials in Smart Structures. *Computational Methods in Science and Technology, 10*(2), pp. 147–160.

Herrera-Mesen, C., Salvador, R. P., Cavalaro, S., & Aguado, A. (2019). Effect of gypsum content in sprayed cementitious matrices: Early age hydration and mechanical properties. *Cement and Concrete Composites, 95*, pp. 81–91.

Keulen, A., Yu, Q. L., Zhang, S., & Grünewald, S. (2018). Effect of admixture on the pore structure refinement and enhanced performance of alkali-activated fly ash-slag concrete. *Construction and Building Materials, 162*, pp. 27–36.

Lavergne, F., Belhadi, R., Carriat, J., & Ben Fraj, A. (2019). Effect of nano-silica particles on the hydration, the rheology and the strength development of a blended cement paste. *Cement and Concrete Composites, 95*, pp. 42–55.

Li, L. G., Lin, C. J., Chen, G. M., Kwan, A., & Jiang, T. (2017). Effects of packing on compressive behaviour of recycled aggregate concrete. *Construction and Building Materials, 157*, pp. 757–777.

Li, T., Chen, Y., Hu, X., Li, Y., & Wang, L. (2018). Exploiting negative Poisson's ratio to design 3D-printed composites with enhanced mechanical properties. *Materials & Design, 142*, pp. 247–258.

Lim, T.-C. (2015). *Auxetic Materials and Structures.* Singapore: Springer Singapore.

Wikipedia (Ed.). (2021). *Local regression*. Retrieved 10 7, 2021, from https://en.wikipedia.org/w/index.php?title=Local_regression&oldid=1029637107

McCormick, N., & Lord, J. (2010). Digital Image Correlation. *Materials Today, 13*(12), pp. 52–54.

Mehta, P. K., & Monteiro, P. J. (2014). *Concrete* (4. ed. ed.). New York, NY: McGraw-Hill Education.

Mir, M., Ali, M. N., Sami, J., & Ansari, U. (2014). Review of Mechanics and Applications of Auxetic Structures. *Advances in Materials Science and Engineering, 2014*, pp. 1–17.

Mishra, G. (n.d.). Why do We Test Concrete Compressive Strength after 28 Days?

Moini, M., Olek, J., Youngblood, J. P., Magee, B., & Zavattieri, P. D. (2018). Additive Manufacturing and Performance of Architectured Cement-Based Materials. *Advanced materials (Deerfield Beach, Fla.), 30*(43), p. e1802123.

Özcan, F., & Emin Koç, M. (2018). Influence of ground pumice on compressive strength and air content of both non-air and air entrained concrete in fresh and hardened state. *Construction and Building Materials, 187*, pp. 382–393.

Qiao, M., Chen, J., Yu, C., Wu, S., Gao, N., & Ran, Q. (2017). Gemini surfactants as novel air entraining agents for concrete. *Cement and Concrete Research, 100*, pp. 40–46.

Rahmouni, I., Promis, G., R'mili, A., Beji, H., & Limam, O. (2019). Effect of carbonated aggregates on the mechanical properties and thermal conductivity of eco-concrete. *Construction and Building Materials, 197*, pp. 241–250.

Ren, X., Das, R., Tran, P., Ngo, T. D., & Xie, Y. M. (2018). Auxetic metamaterials and structures: a review. *Smart Materials and Structures, 27*(2), p. 023001.

Savastano, H., Santos, S. F., Radonjic, M., & Soboyejo, W. O. (2009). Fracture and fatigue of natural fiber-reinforced cementitious composites. *Cement and Concrete Composites, 31*(4), pp. 232–243.

Savija, B. (2020). Use of 3D printing to create multifunctional cementitious composites: review, challenges and opportunities. *RILEM Technical Letters, 5*, pp. 17–25.

Subramani, P., Rana, S., Ghiassi, B., Fangueiro, R., Oliveira, D. V., Lourenco, P. B., & Xavier, J. (2016). Development and characterization of novel auxetic structures based on re-entrant hexagon design produced from braided composites. *Composites Part B: Engineering, 93*, pp. 132–142.

Sun, Y., Wang, Z., Gao, Q., & Liu, C. (2018). A new mixture design methodology based on the Packing Density Theory for high performance concrete in bridge engineering. *Construction and Building Materials, 182*, pp. 80–93.

T Zahra. (2019). Role of Auxetic Composites in Protection of Building Materials and Structures.

Test Method for Compressive Strength of Hydraulic Cement Mortars (Using 2-in. or [50-mm] Cube Specimens). (2020). *(ASTM C109/C109M - 20b)*. West Conshohocken, PA.

Test Method for Flexural Strength of Concrete (Using Simple Beam with Third-Point Loading). (2021). *(ASTM C78/C78M - 21)*. West Conshohocken, PA.

TU Delft. (n.d.). *Obtaining energy from concrete*. Retrieved 12 7, 2021, from https://www.tudelft.nl/en/2021/citg/obtaining-energy-from-concrete

Wongchai, B. (2021). AUXETIC TWO-DIMENSION MATERIAL WITH MODIFIED PEANUT PATTERN. *International Journal of GEOMATE, 20*(79).

Xu, Y., Schlangen, E., Luković, M., & Šavija, B. (2021). Tunable mechanical behavior of auxetic cementitious cellular composites (CCCs): Experiments and simulations. *Construction and Building Materials, 266*, p. 121388.

Xu, Y., Zhang, H., Schlangen, E., Luković, M., & Šavija, B. (2020). Cementitious cellular composites with auxetic behavior. *Cement and Concrete Composites, 111*, p. 103624.

Yanping Liu, & Hong Hu. (2010). A review on auxetic structures and polymeric materials. *Scientific Research and Essays, 5*(10), pp. 1052–1063.

Yoo, D.-Y., & Banthia, N. (2016). Mechanical properties of ultra-high-performance fiber-reinforced concrete: A review. *Cement and Concrete Composites, 73*, pp. 267–280.

Yoon, J. Y., & Kim, J. H. (2019). Mechanical properties of preplaced lightweight aggregates concrete. *Construction and Building Materials, 216*, pp. 440–449.

Zhou, H., Jia, K., Wang, X., Xiong, M.-X., & Wang, Y. (2020). Experimental and numerical investigation of low velocity impact response of foam concrete filled auxetic honeycombs. *Thin-Walled Structures, 154*, p. 106898.